THESIS APPROVAL

GRADUATE SCHOOL, KASETSART UNIVERSITY

Master of Engineering (Chemical Engineering)

DEGREE

Chemical Engineering	Chemical Engineering
FIELD	**DEPARTMENT**

TITLE: Ni/ZSM-5-SBA-15 Composites Catalyst for Carbon Dioxide Hydrogenation with Methane

NAME: Mr. Thammachat Metchanan

THIS THESIS HAS BEEN ACCEPTED BY

THESIS ADVISOR

(Associate Professor Metta Chareonpanich, D.Eng.)

THESIS CO-ADVISOR

(Associate Professor Phungphai Phanawadee, D.Sc.)

DEPARTMENT HEAD

(Associate Professor Apinya Duangchan, Ph.D.)

APPROVED BY THE GRADUATE SCHOOL ON _____

DEAN

(Associate Professor Gunjana Theeragool, D.Agr.)

THESIS

Ni/ZSM-5−SBA-15 COMPOSITES CATALYST FOR CARBON DIOXIDE HYDROGENATION WITH METHANE

THAMMACHAT METCHANAN

A Thesis Submitted in Partial Fulfillment of
the Requirements for the Degree of
Master of Engineering (Chemical Engineering)
Graduate School, Kasetsart University
2011

Thammachat Metchanan 2011: Ni/ZSM-5−SBA-15 Composites Catalyst for Carbon Dioxide Hydrogenation with Methane. Master of Engineering (Chemical Engineering), Major Field: Chemical Engineering, Department of Chemical Engineering. Thesis Advisor: Associate Professor Metta Chareonpanich, D.Eng. 92 pages.

ZSM-5 zeolite and SBA-15 mesoporous silica exhibits the great performance when used as catalyst supports for various kind of applications because of their unique structures. However, their drawbacks were also reported when used as supports for Ni/ZSM-5 and Ni/SBA-15 catalysts in CO_2 reforming of CH_4 reaction. The microporous structure of ZSM-5 zeolite generally leads the catalysts to deactivate by carbonaceous species and aggregated Ni metals on the surface of the catalyst, while SBA-15 mesoporous silica requires very high operating temperature to obtain its best performance. Therefore, ZSM-5−SBA-15 composites support comprised of good advantages of ZSM-5 zeolite and SBA-15 mesoporous silica was synthesized and investigated for various factors that affected to its structure and morphology. Then, it was used as the support for Ni loading in CO_2 reforming of CH_4 reaction. It was found that in order to obtain the complete structure of ZSM-5 zeolite in ZSM-5−SBA-15 composites, at least 7 h of the hydrothermal treatment time period was required. The template and high acid condition of SBA-15 mesoporous silica synthesis did not affect on the structure of ZSM-5 zeolite. The smaller size of ZSM-5 zeolite seeding, more uniform structure of ZSM-5−SBA-15 composites was obtained. Moreover, Ni/ZSM-5−SBA-15 catalyst exhibited the highest performance in CO_2 hydrogenation with CH_4 compared to those of Ni/ZSM-5 and Ni/SBA-15 catalysts due to the advantages of ZSM-5 zeolite and SBA-15 mesoporous silica in its structure.

_____ _____ ___ / ___ / ___

Student's signature Thesis Advisor's signature

ACKNOWLEDGEMENTS

I would like to express my sincere gratitude to my advisor, Associate Professor Metta Chareonpanich, for her guidance, invaluable suggestion and support throughout this research. I am very thankful to Associate Professor Phungphai Phanawadee for his kindly giving the time to revise and approve my thesis.

I am grateful for the financial support from the Kasetsart University Research and Development Institute (KURDI), Nanotechnology Center of Kasetsart University, and National Center of Excellence for Petroleum, Petrochemicals and Advanced Materials (PPAM). The Graduate School of Kasetsart University is also acknowledged.

I would like to thank for the help of my senior research colleagues and for the assistance and valuable suggestion from administrative staffs and technical staffs at Department of Chemical Engineering, Kasetsart University. The kind assistance of characterization and measurement from the staffs at National Metal and Materials Technology Center (MTEC), and Office of Atoms for Peace (OAP) are admirably acknowledged.

Finally, I have a lot to be thankful to my family and for their adoration, support, encouragement, and their understanding during the whole period of my education.

Thammachat Metchanan

April 2011

TABLE OF CONTENTS

Page

LIST OF TABLES

LIST OF FIGURES

LIST OF FIGURES (Continued)

LIST OF FIGURES (Continued)

LIST OF ABBREVIATIONS

ºC	=	Degree Celsius
Å	=	Angstrom
BET	=	Brunauer-Emmett-Teller
GC	=	Gas Chromatograph
GHSV	=	Gas Hourly Space Velocity
g_{cat}	=	Gram of Catalyst
HK	=	Horvath–Kawazoe
h	=	Hour
kPa	=	Kilo Pascal
M	=	Molar
MCM-41	=	Mobil Composition of Matter No. 41
mA	=	Milli Ampare
mL	=	Milliliter
mg	=	Milligram
Ni	=	Nickel
nm	=	Nanometer
P	=	Pressure
RWGS	=	Reverse Water Gas Shift
SANS	=	Small Angle Neutron Scattering
SAXS	=	Small Angle X-ray Scattering
SBA-15	=	Santa Barbara Amorphous Silica No. 15
SEM	=	Scanning Electron Microscopy
STP	=	Standard Temperature and Pressure
T	=	Temperature
TCD	=	Thermal Conductivity Detector
TEM	=	Transmission Electron Microscopy
TGA	=	Thermogravimetric Analysis
wt. %	=	Percent by weight
ZSM-5	=	Zeolite Socony Mobil No.5

Ni/ZSM-5–SBA-15 COMPOSITES CATALYST FOR CARBON DIOXIDE HYDROGENATION WITH METHANE

INTRODUCTION

Nowadays, many attentions have been focused on the lack of fossil energy and global warming problems caused by greenhouse effect due to greenhouse gases emissions from exhaust gases of industrial processes and transportation, resulted in the increase of global temperature.

In order to reduce these problems, many researchers focused on the ways to decrease greenhouse gases. Therefore, reforming processes that used major greenhouse gases (CH_4 or CO_2) to produce synthesis gas (CO and H_2), the valued primary reactants used for alternative energy source production as the product are of great interest.

Generally, reforming processes could be classified by the reactants used such as steam reforming (CH_4 and H_2O), methane partial oxidation (CH_4 and O_2) and dry reforming (CH_4 and CO_2). Comparing between these processes, dry reforming is concerned as a suitable process for greenhouse gases utilization. It produces synthesis gas with a low H_2/CO ratio which is appropriate for the synthesis of oxygenated chemicals and production of high-purity CO. However, the main problem of dry reforming is that the highly endothermic reaction nature (Edwards and Maitra, 1995; Wang *et al.*, 1996). Moreover, high operating temperature of this reaction leaded to the deactivation of catalysts by coking or loss of active sites. To minimize this problem, the catalyst and reaction condition are the two main factors that must be considered. In the literature review, it was found that the catalyst activity and stability were affected by many variables, i.e., types of metal, support, and catalyst preparation technique. Generally, the catalysts based on noble metals were reported to show high activity with low sensitivity to coke formation (Zhang *et al.*, 1996; Mark and Maier, 1996; Bradford and Vannice, 1998). However, considering the aspects of high cost and limited availability of those noble metals, it was more practical to search for the

other available metals which had similar characteristics. Therefore, non-noble metals, especially Ni were numerous studied (Edwards and Maitra, 1995; Wang and Lu, 1998). Although Ni-based catalysts gave high activity similar to the noble metal based catalysts, the deactivation problem of these catalysts were significantly found due to coke formation.

The support was an essential factor affecting the performance of the catalysts. Zeolite support which contained high surface area, surface acidity and thermal stability revealed a high activity as the reforming support (Li *et al.*, 1998; Solymisi *et al.*, 1999; Halliche *et al.*, 2007). Luengnaruemitchai and Kaengsilalai (2008) compared the dry reforming activity among many structures of zeolites. ZSM-5 zeolite and zeolite Y had the better activity than zeolite A and zeolite X. Considering between ZSM-5 zeolite and zeolite Y, the very high acidity of zeolite Y caused by low ratio of Si/Al leading to coke formation which was the major problem for the catalyst stability. Therefore, the lower acidity of ZSM-5 zeolite from its higher Si/Al ratio gave the advantage for catalyst stability. However, microporous structure of ZSM-5 zeolite was the main drawback due to the deactivation of catalyst caused by aggregated metal and carbonaceous species form during the reaction. Therefore, the methods to modify the porous structure of ZSM-5 zeolite such as desilication (Groen *et al.*, 2006), carbon templating (Schüth, 2003; Kustova *et al.*, 2007), and supramolecular templating (Freyhardt *et al.*, 1996; Corma *et al.*, 2002, 2004, 2006) were concerned, in order to obtain ZSM-5 zeolite with hierarchical porous structure. For supramolecular templating method, the ordered mesoporous silica such as MCM-41, MCM-48 and SBA-15 were used (Campos *et al.*, 2006 and Ogura et al., 2006). Comparing between these mesoporous silica, SBA-15 mesoporous silica was preferable to combine with ZSM-5 zeolite because of its great hydrothermal stability. However, the synthesis conditions of SBA-15 mesoporous silica and ZSM-5 zeolite were significantly different since SBA-15 mesoporous silica was synthesized in acidic condition, while ZSM-5 zeolite was synthesized in basic condition.

In this research, the ZSM-5–SBA-15 composites with microporous structure of ZSM-5 zeolite and the mesoporous structure of SBA-15 mesoporous silica were synthesized. The effect of amount of ZSM-5 zeolite seeding, Pluronic P123, the

adding sequence and hydrothermal treatment time periods of ZSM-5 zeolite seeding on the structure and morphology of ZSM-5–SBA-15 composites were investigated. Then, Ni metal was loaded onto the ZSM-5 zeolite, SBA-15 mesoporous silica and ZSM-5–SBA-15 composites supports by using wet impregnation technique. The catalytic performance for CO_2 hydrogenation with CH_4 over Ni/ZSM-5–SBA-15 catalyst was investigated and compared to those of Ni/ZSM-5 and Ni/SBA-15 catalysts.

OBJECTIVES

1. To synthesize ZSM-5 zeolite, SBA-15 mesoporous silica and ZSM-5–SBA-15 composites.

2. To study the effect of amount of ZSM-5 zeolite seeding, Pluronic P123, the adding sequence and hydrothermal treatment time periods of ZSM-5 zeolite seeding on the structure and morphology of ZSM-5–SBA-15 composites.

3. To investigate and compare the catalytic performance for CO_2 hydrogenation with CH_4 over Ni/ZSM-5–SBA-15 catalyst to those of Ni/ZSM-5 and Ni/SBA-15 catalysts.

Benefits

1. ZSM-5–SBA-15 composites comprised of microporous structure of ZSM-5 zeolite and mesoporous structure of SBA-15 mesoporous silica was successfully synthesized.

2. The factors affecting the structure and morphology of ZSM-5–SBA-15 composites were observed and the synthesis condition was also revealed.

3. Ni/ZSM-5–SBA-15 catalyst exhibited the highest performance in CO_2 hydrogenation with CH_4 due to the advantages of ZSM-5 zeolite and SBA-15 mesoporous silica in its structure.

LITERATURE REVIEW

Zeolite–mesoporous silica composites materials have several applications including catalysis, adsorption, and selective separation, where both molecular transportation and interaction between solid surface and molecules could be occurred simultaneously. These composites comprised of two different pore sizes; the microporous surface from zeolite could interact with molecules while the mesoporous provide more transport of fluid in reaction (Corma, 1997; Tao *et al.*, 2006; Pérez-Ramírez *et al.*, 2008). CO_2 hydrogenation with CH_4 has been the promising syngas production process that uses two important greenhouse gases as reactants (Edwards and Maitra, 1995; Wang *et al.*, 1996; Lu and Wang, 1999). Many works have focused on investigations of conditions and catalysts suitable for this process and enable to apply for industrial scale.

The detail of background information regarding CO_2 hydrogenation with CH_4 reaction and zeolite-mesoporous silica composites synthesis were shown as follows.

1. Syngas production

Recently, synthesis gas has been attracted for industrial process because it is the primary reactant for alternative energy sources production (Balat *et al.*, 1996). The synthesis gas is the gas mixture of carbon monoxide (CO) and hydrogen (H_2) mainly obtained from some processes such as steam reforming, partial oxidation and CO_2 hydrogenation with CH_4 as shown in following reaction

1) Steam reforming (Bengaard *et al.*, 2002; Didenko *et al.*, 2008)

$$CH_4 + H_2O \rightarrow CO + 3H_2 \qquad \Delta H^0_{298} = 206 \text{ kJ/mol} \qquad (1)$$

2) Partial oxidation of methane (Hu and Ruckenstein, 1996; Au and Wang, 1997; Tsipouriari and Verykios, 1998)

$$2CH_4 + O_2 \rightarrow 2CO + 4H_2 \qquad \Delta H^0_{298} = -71 \text{ kJ/mol} \qquad (2)$$

3) Dry reforming (Edwards and Maitra, 1995; Wang *et al*., 1996; Lu and Wang, 1999)

$$CH_4 + CO_2 \rightarrow 2CO + 2H_2 \qquad \Delta H^0_{298} = 247 \text{ kJ/mol} \qquad (3)$$

From Eq.1, the disadvantage of steam reforming is occurred by poor selectivity of CO showed in too much H_2/CO ratio of the syngas product which does not match for the use as the reactant to produce oxygenated chemicals (Wang *et al*., 1996). The partial oxidation reaction of methane in Eq.2 provides high methane conversion with lower H_2/CO ratio of syngas product than that of steam reforming. However, its exothermic reaction leads to produce a large amount of heat which is difficult to remove from the catalyst zone. Therefore, this process is concerned to be very hazardous and difficult to control in the industrial or large scale operation. Considering another syngas production process, dry reforming has lower H_2/CO ratio of syngas product and available waste greenhouse gases also used as reactants. Therefore, this process has become a promising industrial process (Edwards and Maitra, 1995; Wang *et al*., 1996; Lu and Wang, 1999).

2. CO_2 hydrogenation with CH_4

CO_2 hydrogenation with CH_4 that consists of dry reforming reaction is the one of major routes to produce synthesis gas (CO and H_2) which has been used as reactants for produce many worthy hydrocarbon substances with two major advantages. First, this process uses two important greenhouse gases (CH_4 and CO_2) emitted from wastes of industrial processes and transportation as reactants, and moreover, it provides suitable H_2/CO ratio of syngas product for the use as reactants in oxygenated chemicals production. Normally, this process was very high endothermic, the catalysts have been applied in order to decrease the operating

temperature and increase process activity. The details of this reaction and catalysts used were described as follows.

2.1 Catalysts in CO_2 hydrogenation with CH_4

In CO_2 hydrogenation with CH_4, the catalyst is the important part that affected the performance of catalyst both activity and performance. Basically, transition metals group VIII, especially Rhodium (Rh) or Iridium (Ir) were applied and reported higher activity with greater stability as shown in Table 1.

Table 1 CH_4 and CO_2 conversion in CO_2 hydrogenation with CH_4 on different metals with Al_2O_3 support

Catalyst	Conversion (%)	
	CH_4	CO_2
Pd	71	75
Ru	67	71
Rh	86	88
Ir	88	91

Condition: CO_2/CH_4, 1/1; temperature, 777°C; pressure, 1 atm; reactor, fixed-bed; metal loading, 1wt%

Source: Ashcroft *et al.* (1991)

Although Rh and Ir were reported to give higher activity with greater stability, they is noble metals and very expensive for the use in the industrial scale. Therefore, comparing to the non-noble metals in transition group VIII, Ni metal also provided high activity similar to the noble metal as shown in Table 2. It has been regarded as the most promising catalyst for the use as the metal catalyst in CO_2 hydrogenation with CH_4.

Table 2 CH_4 conversion in CO_2 hydrogenation with CH_4 on different metals with SiO_2 support

Catalyst	CH_4 conversion (%)
Ni	80
Co	66
Fe	2
Mo	15
W	0
Cu	0

Condition: CO_2/CH_4, 1/1; temperature, 850°C; pressure, 1 atm; reactor, fixed-bed; metal loading, 23wt%

Source: Edward and Maitra (1995)

2.2 Mechanism of CO_2 hydrogenation with CH_4 on the surface of catalyst

Many researchers had proposed the mechanisms of CO_2 hydrogenation with CH_4 on catalysts (Edwards and Maitra, 1995; Tang *et al.*, 1995; Mark and Maier, 1996; Wang *et al*., 1996; Tomishige *et al*., 1998, 1999; Aparicio *et al*., 2000; Ginsburg *et al.*, 2005; Cui *et al*., 2007). In conclusion of those works, the main reactions related to mechanism of CO_2 hydrogenation with CH_4 were described as follows.

CH_4 dissociation: $CH_4 + (5-x)*1 \rightarrow CH_x*1 + (4-x)\ H*1$ (4)

$CH_x*1 + *1 \rightleftharpoons CH_{x-1}*1 + H*1$ (5)

CO_2 decomposition: $CO_2 + *1 \rightarrow CO + O*1$ (6)

$CO_2 + *2 \rightarrow CO + O*2$ (7)

Oxidation of CH_x: $CH_x*1 + O*1 \rightarrow CO_2 + (x/2)H_2 + 2*1$ (8)

Reforming reaction: $CH_x*1 + CO_2 + (x+1)*1 \rightarrow 2CO*1 + xH*1$ (9)

CO desorption: $CO*1 \rightarrow CO + *1$ (10)

H_2 desorption: $2H*1 \rightleftharpoons H_2 + 2*1$ (11)

Surface oxygen exchange: $O*2 + *1 \rightarrow O*1 + *2$ (12)

Where *1 refers to metal active sites and *2 refers to support active sites.

As shown in Figure 1, CH_4 firstly dissociated (Eq.4) on the metal surface and produced the surface carbon species (CH_x*1) and hydrogen (H*1), while CO_2 decomposed on both the metal surface and the support surface produced CO as the product gas and surface oxygen (O*1 and O*2) in as shown in Eq.6-7.

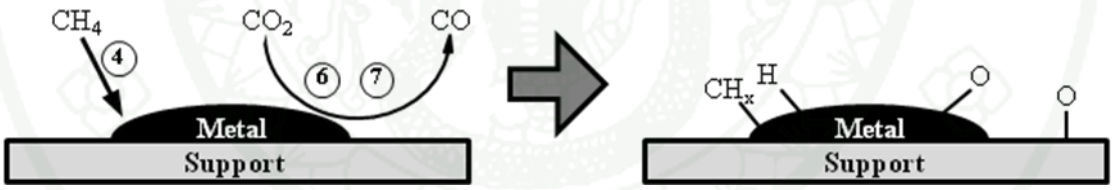

Figure 1 CH_4 dissociation and CO_2 decomposition on Ni metal surface and support.

From Figure 2, the surface carbon species on metal active sites (CH_x*1) obtained from CH_4 dissociation reaction could either dissociate again to produce the lower hydrogen surface carbon species ($CH_{x-1}*1$) as shown in Eq.5 or oxidize with surface oxygen (O*1) to produce CO_2 and H_2 gases as shown in Eq.8.

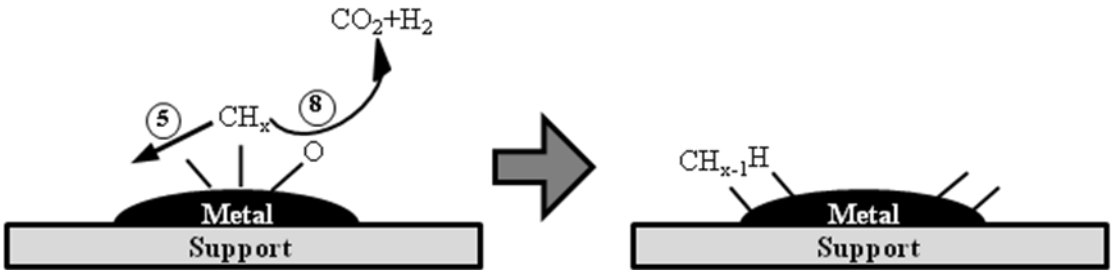

Figure 2 CH_x dissociation and oxidation on metal surface.

Moreover, the surface CO (CO*1) and H (H*1) were obtained by the reforming of the surface carbon species (CH_x*1) and CO_2 gas as the key step of syngas production in CO_2 hydrogenation with CH_4 process as shown in Eq.9.

Figure 3 Reforming reaction on metal surface.

Then, the Ni active sites could regain by the desorption of surface CO (CO*1) and surface H (H*1) in Eq.10-11.

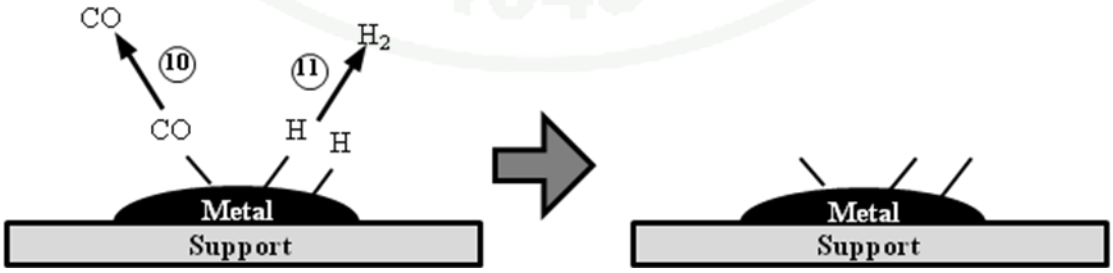

Figure 4 CO and H_2 desorption reaction on metal surface.

In the CO_2 hydrogenation with CH_4, the surface oxygen (O*1) had an important role to remove the surface carbon species (CH_x*1) on the metal surface by oxidation reaction as shown in Eq.8. For Ni-based catalysts, it was reported that Ni metal showed the great activity of CH_4 dissociation, on the other hand, its poor activity in CO_2 decomposition was observed (Panov *et al.*, 1998). Therefore, the surface oxygen was mainly located on support active sites (O*2), but the surface carbon species (CH_x*1) was mainly located in Ni active sites leaded to catalyst deactivation by carbonaceous species formed during reaction. Hence, the surface oxygen on support active sites needed to change the location to the Ni active sites (O*1) as shown in Eq.12 before reacting with the surface carbon species by CH_x oxidation reaction in order to remove carbon species and prevent the aggregation of surface carbon specie on Ni metal. Martin and Duprez (1996) reported that the surface oxygen required sufficient operating temperature to diffuse on the surface of support and exchange active site. From these reasons, the support had important role to control the stability of catalyst.

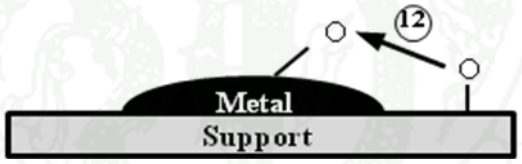

Figure 5 Surface oxygen exchange reaction between metal and support.

In the mechanism of CO_2 hydrogenation with CH_4 as mention above, side reactions including reverse water gas shift (RWGS) and coke formation reaction were not considered. However, due to the fact that side reactions had effects on the performance of main reaction, these side reactions were then taking into account and were described in details as follows.

2.3 Side reaction in CO_2 hydrogenation with CH_4

CO_2 hydrogenation with CH_4 reaction normally has two main side reactions that must be concerned including reverse water gas shift and coke formation reactions because the equilibrium of substance in main reactions is usually affected by these reactions resulting in the change of conversion and product yield.

2.3.1 *Reverse water gas shift (RWGS) reaction*

RWGS reaction in Eq. 13 was the main route for water formation in CO_2 hydrogenation with CH_4 process. This reaction affected the H_2/CO of the product by lower H_2 concentration (Wang *et al*., 1996). Edwards and Maitra (1995) also reported that water came from RWGS reaction contributed to the carbon species removal process as shown in Eq.14.

RWGS reaction: $CO_2 + H_2 \rightarrow H_2O + CO$ (13)

CH_x oxidation with H_2O: $CH_x*1 + H_2O \rightarrow CO + H_2$ (14)

2.3.2 *Coke formation reaction*

In CO_2 hydrogenation with CH_4, the carbon species generated on the catalysts affected the performance of catalyst by decreasing metal active sites or blocking the pores of catalysts, resulting in lower activity and stability of the catalysts which were the major problems in CO_2 hydrogenation with CH_4 process. These carbon species were mainly generated by two ways, CH_4 dissociation shown in Eq.4-5 and Boudouard reactions shown in Eq.15.

CH_4 dissociation: $CH_4 + (5-x)*1 \rightarrow CH_x*1 + (4-x)\ H*1$ (4)

$CH_x*1 + *1 \rightleftharpoons CH_{x-1}*1 + H*1$ (5)

Boudouard reaction: $2CO \rightarrow CO_2 + C$ (15)

To remove these carbon species, the suitable support was required as mention previously. In example, Cui *et al.* (2007) proposed that the active site exchange of the surface oxygen on Ni/α-Al_2O_3 catalyst was occurred at the temperature higher than 575°C. Therefore, the support was also an important factor affecting the performance of CO_2 hydrogenation with CH_4 reaction. The details of the supports for CO_2 hydrogenation with CH_4 reaction were described below.

3. Catalyst support for CO_2 hydrogenation with CH_4

Many researchers had investigated the suitable support to promote the stability of Ni-based catalyst (Lu and Wang, 1999). Al_2O_3 was usually for this purpose. Its high performance as the support for CO_2 hydrogenation with CH_4 was reported as shown in Table 3.

Table 3 CH_4 conversion in CO_2 hydrogenation with CH_4 process on Ni with different support

Support	CH_4 conversion (%)
Al_2O_3	84
SiO_2	79
MgO	71
La_2O_3	82
CeO_2	63
TiO_2	8
Clay	61
Zeolite	73

Condition: CO_2/CH_4, 1/1; temperature, 700°C; pressure, 1 atm; fixed-bed reactor

Source: Lu and Wang (1999)

Although Al_2O_3 was the promising support for CO_2 hydrogenation with CH_4, the other supports such as zeolites, especially ZSM-5 zeolite also showed good performance in this reaction (Luengnaruemitchai and Kaengsilalai, 2008).

Table 4 CH_4 conversion in CO_2 hydrogenation with CH_4 different zeolite-supported Ni catalysts

Catalyst	CH_4 conversion (%)
zeolite A	71
zeolite X	82
zeolite Y	91
ZSM-5	91

Condition: CO_2/CH_4, 1/1; temperature, 700°C; pressure,1 atm; reactor, fixed-bed; Ni loading, 7 wt%

Source: Luengnaruemitchai and Kaengsilalai (2008)

It was reported that the acidity and thermal stability of ZSM-5 zeolite could promote better performance when ZSM-5 zeolite was used as the catalyst (Davis, 1991; Davis and Lobo, 1992; Corma, 1995). However, the microporous structure of ZSM-5 zeolite was easily blocked by carbonaceous species during the reaction, resulting in less stability of ZSM-5 zeolite. Recently, this problem could be solved by promoting the mesoporous silica structure into microporous structure of zeolites (Takahashi *et al.*, 2007). In this work, the microporous structure of ZSM-5 zeolite was modified by SBA-15 mesoporous structure in order to obtain ZSM-5–SBA-15 composites support that comprised of the microporous structure of ZSM-5 zeolite as the as active surfaces for the reaction and mesoporous structure of SBA-15 as the promoter of gas diffusivity and Ni dispersion. In the next section, the background theories of ZSM-5 zeolite, SBA-15 mesoporous silica and ZSM-5–SBA-15 composites supports were explained in details.

3.1 ZSM-5 zeolite

Zeolite is derived from the two Greek words “zeo”, to boil, and “lithos”, stone. The first natural zeolite stilbite (STI) was discovered by Swedish mineralogist, A. F. Cronstedt, in 1756 after heated an unidentified silicate mineral and observed that the mineral fused readily in a blowpipe flame with obvious intumescence. In 1845, Schafhautle reported the preparation of quartz by heating a silicate gel with water in an autoclave under hydrothermal condition. After that, many reports of succeeding zeolite synthesis were come (McCusker and Baerlocher, 2007). For ZSM-5 (Zeolite Socony Mobil No.5), it was firstly discovered by Argauer and Landolt (1972) and classified as a high silica zeolite due to its high Si/Al ratio.

3.1.1 *Structure and properties of ZSM-5 zeolite*

It has been known that zeolites are hydrated, crystalline aluminosilicates constructed from TO_4 tetrahedra via oxygen sharing as shown in Figure 6 (T = tetrahedral atom, e.g., Si and Al).

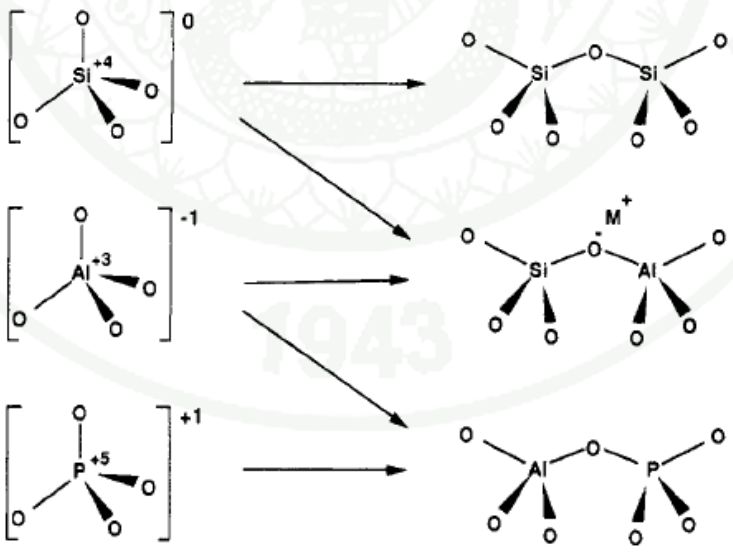

Figure 6 TO_4 units in zeolites and aluminophosphates.

Source: Davis (1991)

For ZSM-5 zeolite, it is generated from pentasil units of connected TO_4 tetrahedra, these units were linked to create pentasil chain. The chain was connected with another via oxygen bridges formed the corrugated sheets of 3-dimensional structure with 10-ring holes (e.g., the gray sheet in Figure 7).

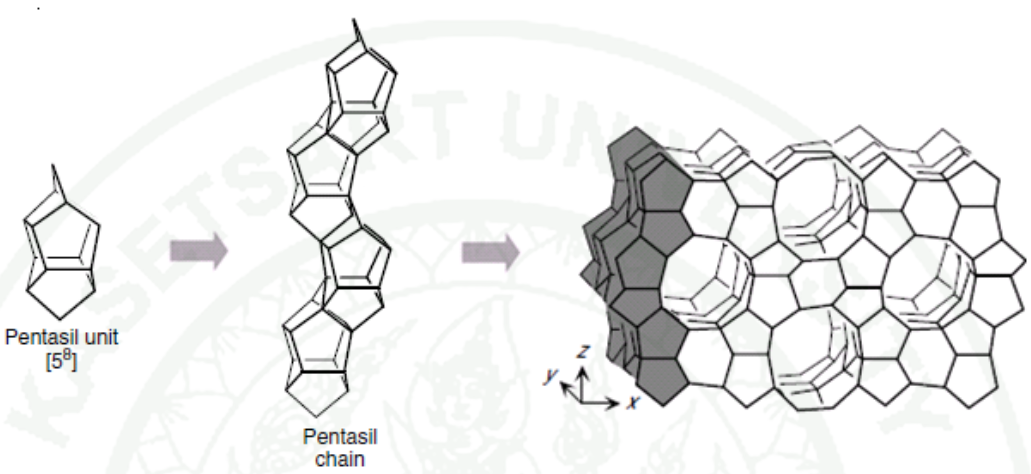

Figure 7 The creation of ZSM-5 zeolite framework from pentasil units.

Source: McCusker and Baerlocher (2007)

Due to the fact that the 3-dimensional structure with 10-ring of ZSM-5 zeolite is wide enough to absorb molecules up to only 0.6 nm in diameter. It provides different shape selectivity for sorption and catalysis from the others types of zeolites. This fact causes ZSM-5 zeolite has been found in many refinery and petrochemical processes applications (McCusker and Baerlocher, 2007**)**. Moreover, its ion-exchange ability and acidity provided from the cation sites, and thermal stability provided from the crystal structure has been attracted many researchers to investigate (Davis, 1991; Davis and Lobo, 1992; Corma, 1995).

3.1.2 *Synthesis of ZSM-5 zeolite*

Recently, many ZSM-5 synthesis conditions were reported (Panpa and Jinawath, 2009). It could be concluded that the 3 main components in ZSM-5 synthesis were consisted of the silica source, alumina source and structure directing

agent. Based on Chareonpanich *et al.* (2004), ZSM-5 zeolite (shown in Figure 8) was obtained by following conditions: SiO_2/Al_2O_3 mole ratio, 40; the holding temperature, 210 °C; the holding time, 4 h and the initial pressure, 4 bars.

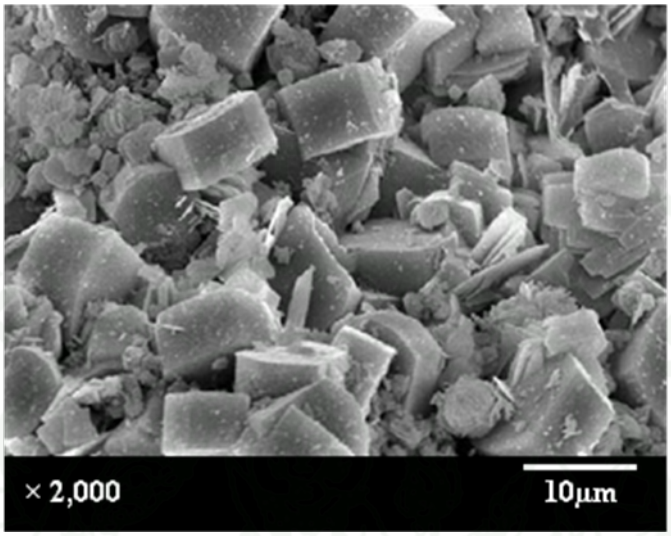

Figure 8 SEM photographs of treated products obtained from synthesis at holding temperatures of 210 °C (SiO_2/Al_2O_3 mole ratio: 40).

Source: Chareonpanich *et al.* (2003)

Until now there was no complete understanding how amorphous gels were converted to the porous crystalline products in the mechanism of ZSM-5 synthesis because of the complex chemical reactions and equilibria between solid and solution components involved in the crystallization process (Yu, 2007). In 1991, Chang and Bell proposed possible mechanism of MFI nucleation on the basis of hydrophobic effect and isomorphism between water and silicate structures which was as follows: (I) formation of clathrate-like water structure around the template; (II) isomorphous substitution of silicate for water in these clathrates; and (III) progressive ordering of these entities into the final crystal structure (Chang and Bell, 1991). This mechanism was later modified by Burkett and Davis (1994, 1995). They investigated the role of TPA^+ during synthesis of MFI type zeolite and proposed that the existence of preorganized inorganic-organic composite precursors in which TPA+ ions were incorporated in an environment similar to the final zeolite. The assembly of

inorganic-organic composite precursors was initiated by overlap of the hydrophobic hydration spheres of the inorganic and organic components, with subsequent release of ordered water, enabling the establishment of favorable van der Waals interactions. Nucleation was assumed to result from aggregation of these composite species, and further crystal growth was suggested to occur through diffusion of the same species to the growing surface, essentially resulting in a layer-by-layer growth pathway as shown in Figure 9.

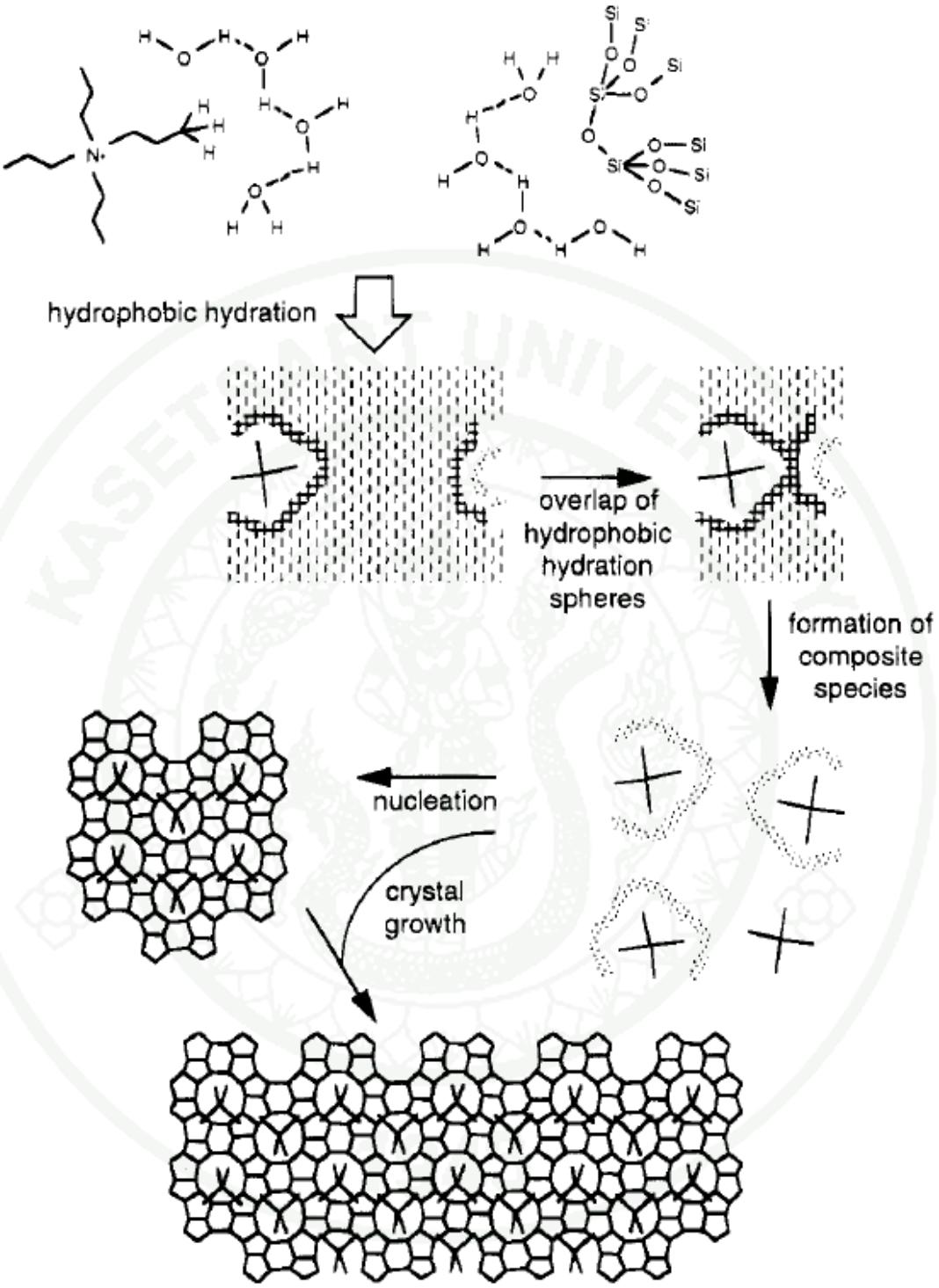

Figure 9 Proposed mechanism of structure direction in the TPA-mediated synthesis of Si-ZSM-5.

Source: Burkett and Davis (1995)

3.2 SBA-15 Mesoporous Silica Support

Periodic mesoporous silica has attracted many researchers to use as catalyst support materials, especially MCM-41 and SBA-15 which were known as the most common types of mesoporous silica. Their properties such as narrow and adjustable pore-size, high surface area and pore volume made them suitable as the supports for catalysts (Zhao *et al.,* 1998; Zholobenko *et al.,* 2001).

3.2.1 *Structure and properties of SBA-15 mesoporous silica*

Comparing between SBA-15 and MCM-41 mesoporous silica, SBA-15 mesoporous silica could provided larger adjustable pore size (from 2 to 30 nm) by using various swelling agents or controlling reaction conditions (Corma, 1997; Zhao *et al.* 1998; Zholobenlo *et al.* 2001). In addition, the unique properties of SBA-15 mesoporous silica such as thick pore wall, 2D hexagonal pore-arrangement, and uniform structure have attracted great attention for large number of applications in catalysis and separation (Guari *et al.,* 2001; Konya *et al.,* 2002; Mirji *et al.,* 2007). Its large surface area (~1,000 m^2/g) and narrow pore size distribution represented the good performance for catalytic reaction. In addition, the thick pore wall of SBA-15 mesoporous exhibited the high thermal stability assisting the preservation of its structure during high temperature process such as drying, calcinations or high temperature reaction (Khodakov *et al.,* 2005).

3.2.2 *Synthesis of SBA-15 mesoporous silica*

The conventional method for prepare SBA-15 mesoporous silica was presented by Nanta-ngern *et al.* (2005). From the rice husk ash silica source, the synthesis condition was controlled under strong acidic condition using Pluronic P123 as the structure-directing agent. The molar ratio of SiO_2: Pluronic P123: H_2O: HCl of 1: 0.0875: 200: 4 was used. The high ordered pore structure of SBA-15 (shown in Figure 10) was obtained after passing the hydrolysis-condensation temperature of 40°C for 24 h and hydrothermal aging temperature of 100°C for 24 h.

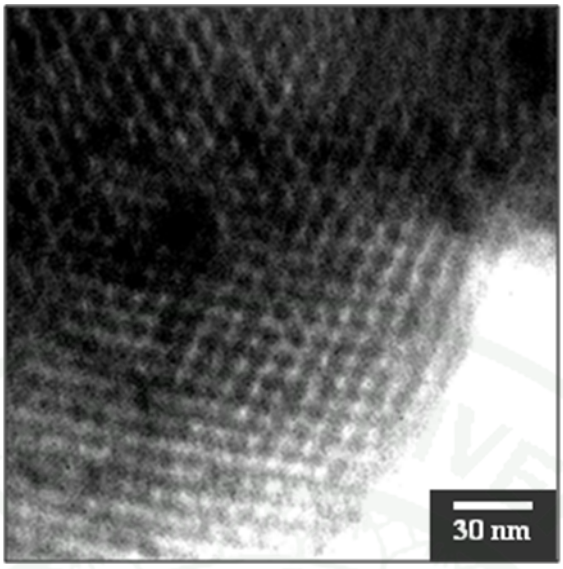

Figure 10 TEM image of SBA-15 synthesized at the SiO_2: Pluronic P123: H_2O: HCl molar ratio of 1: 0.0875 : 200 : 4

Source: Nanta-ngern *et al.* (2005)

After that, the sonication technique was applied in the stage of SBA-15 mesoporous silica synthesis following the procedure reported by Chareonpanich *et al.* (2007). Comparing between conventional and sonication method, the sonication method could decrease synthesis time periods from 24 h to 3-6 h and also enhance the properties and uniformity of SBA-15 mesoporous.

The steps of synthesis procedure of SBA-15 mesoporous silica were investigated by Zholobenko *et al.* (2008) through Synchrotron-based Small Angle X-ray Scattering (SAXS) and Small Angle Neutron Scattering (SANS) techniques. The synthesis mixture was characterized during the reaction of SBA-15 mesoporous silica synthesis. The evolution of the ordered mesoporous silica during SBA-15 mesoporous silica synthesis was monitored and the results confirmed that the formation of SBA-15 proceeded according to the cooperative self-assembly mechanism. Through the hydrolysis and condensation reaction, three major stages in the synthesis of SBA-15 mesoporous silica were identified as shown in Figure 11.

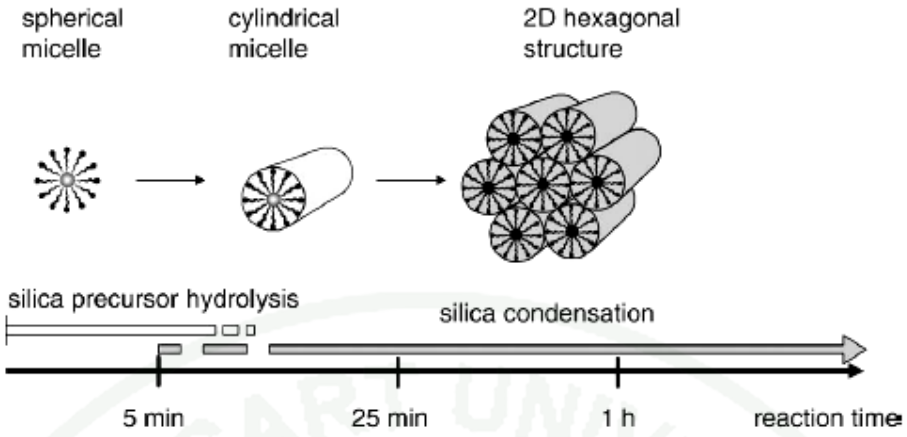

Figure 11 Three initial stages of the evolution of the ordered mesoporous silica during SBA-15 mesoporous silica synthesis.

Source: Zholobenko *et al.* (2008)

During the first stage of synthesis, only spherical micelles of polyethylene oxide-polypropylene oxide-polyethylene oxide (PEO-PPO-PEO) block copolymer were presented in the synthesis mixture, within the first 5 minutes of the reaction. The PPO (polypropylene oxide units) hydrophobic blocks made up the inner micelle core and the PEO (polyethylene oxide units) hydrophilic blocks interacting with water molecules and silicate species represented the micelle corona; in the synthesis mixture, these micelles were surrounded by an aqueous solution of hydrochloric acid. In the second stage, between 5 and 20 minutes of the reaction period, the formation of hybrid organic-inorganic micelles was observed accompanied with the transformation from spherical to cylindrical micelles. The precipitation of the ordered SBA-15 was taken place during the third stage. These micelles began to aggregate into a two-dimensional hexagonal structure confirming that the precipitation occurred as the result of self-assembly of hybrid cylindrical micelles into the structure of SBA-15 mesoporous silica. In the hexagonal matrix, the cylinders were weakly linked initially by the corona. As the synthesis proceeded, the voids between the cylinders were filled with silica species and further condensation reaction resulted in cross-linking and covalent bonding between coronas of the cylindrical micelles. Then, the condensation of silica species continued for the reaction duration

of about 20 h, at 40°C. In this stage, the diameter of the inner core of the obtained SBA-15 structure remained equal to the diameter of the PPO core in the surfactant-silicate cylindrical micelles. Subsequently, the synthesis mixture exposed to the higher temperature typically 80-100°C under hydrothermal condition and about 500°C during calcination. It led to further condensation and densification of the structure with an increase of pore size, resulting in the formation of highly ordered and thermally stable SBA-15 mesoporous phase.

3.3 ZSM-5–SBA-15 composites

As mentioned above, ZSM-5 provided high ability in CH_4 cracking, CO_2 adsorption and surface oxygen exchange reaction leading to the high activity for CO_2 hydrogenation with CH_4 reaction. However, the low performance in CO_2 hydrogenation with CH_4 reaction of Ni/ZSM-5 catalyst was caused by its microporous structure. For Ni/SBA-15 catalyst, it was reported that the surface oxygen required high temperature (>650°C) to diffuse on the surface and exchange active site with Ni metal (Martin and Duprez, 1996) resulting in the high operating temperature (>650°C) was needed in order to exhibit the maximum performance of Ni/SBA-15 catalyst for CO_2 hydrogenation with CH_4 reaction. Therefore, ZSM-5–SBA-15 composites which combined the advantage of ZSM-5 zeolite and SBA-15 mesoporous silica was considered.

3.3.1 Structure and properties of ZSM-5–SBA-15 composites support

Nowadays, the 4 different main types of modified zeolites was reported by Pérez-Ramírez *et al.* (2008) as shown in Figure 12: (I) wide-pore zeolites which had substantially wider micropores than regular zeolite structures, (II) nanosized zeolites which had intercrystalline mesopore, (III) zeolite composites which was zeolite crystals supported on a material that was typically mesoporous or macroporous, and (IV) mesoporous zeolite crystals which exhibited intracrystalline mesopores in the structure.

According to the nature of their porosity, these materials could be categorized into two different groups: (a) unimodal pore system which only had well-defined intracrystalline micropores in the structure, and (b) hierarchical pore systems which had both well-defined intracrystalline micropores and larger pores from either intercrystalline or intracrystalline.

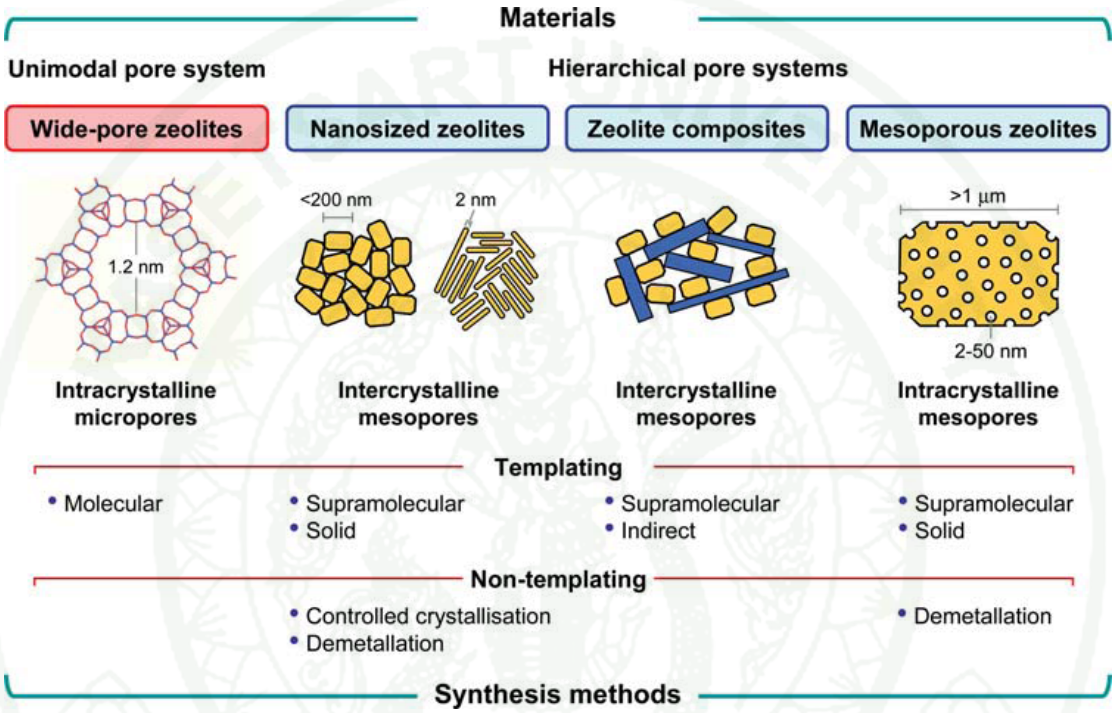

Figure 12 Type of modified zeolites.

Source: Pérez-Ramírez *et al.* (2008)

For ZSM-5–SBA-15 composites used in this work, it was classified into zeolite composites with hierarchical porous system that consisted of microporous structure from ZSM-5 zeolite and mesoporous structure from SBA-15 mesoporous silica. This structure is proposed to promote the activity for CO_2 hydrogenation with CH_4 reaction and in the same time lessen the catalyst deactivation problem from nickel aggregation due to the existences of ZSM-5 zeolite and SBA-15 mesoporous silica structures, respectively.

3.3.2 Synthesis of ZSM-5–SBA-15 composites support

Pérez-Ramírez *et al.* (2008) also reported that the synthesis methods of composites materials were separated into 2 main methods including non-templating and templating method.

For non-templating method, two classes could be discerned: (a) demetallation which extracted some metallic from the zeolite framework i.e. silica or alumina (Groen *et al.*, 2006), and (b) controlled crystallization which modified synthesis method to control zeolite crystal sizes such as adding growth inhibitors, increasing the supersaturation, or quenched crystallization (Lin and Yates, 2005).

For templating method, three classes could be discerned: (a) solid templating which solid templates such as porous carbons, resins organic aerogels or polymers were used to control mesopore formation during zeolite crystallization (Schüth, 2003; Kustova *et al.*, 2007), (b) supramolecular templating which surfactant molecules were used to actively direct the synthesis of large micropores or mesopores (Freyhardt *et al.*, 1996; Corma *et al.*, 2002, 2004, 2006), and (c) indirect templating which a preformed template mesoporous material as either (partially) transformed into a mesoporous zeolite material or applied as a supporting material were used for controlling the deposition of zeolite crystals (Čejka and Mintova, 2007; Meynen *et al.*, 2007). In contrast of supramolecular templating method, this method used zeolite seeds with the particle size of 10-50 nm to promote the formation of micro-mesoporous composites. The zeolite seeds were used as the building blocks for self-organization in the mesoporous matrices as shown in Figure 13.

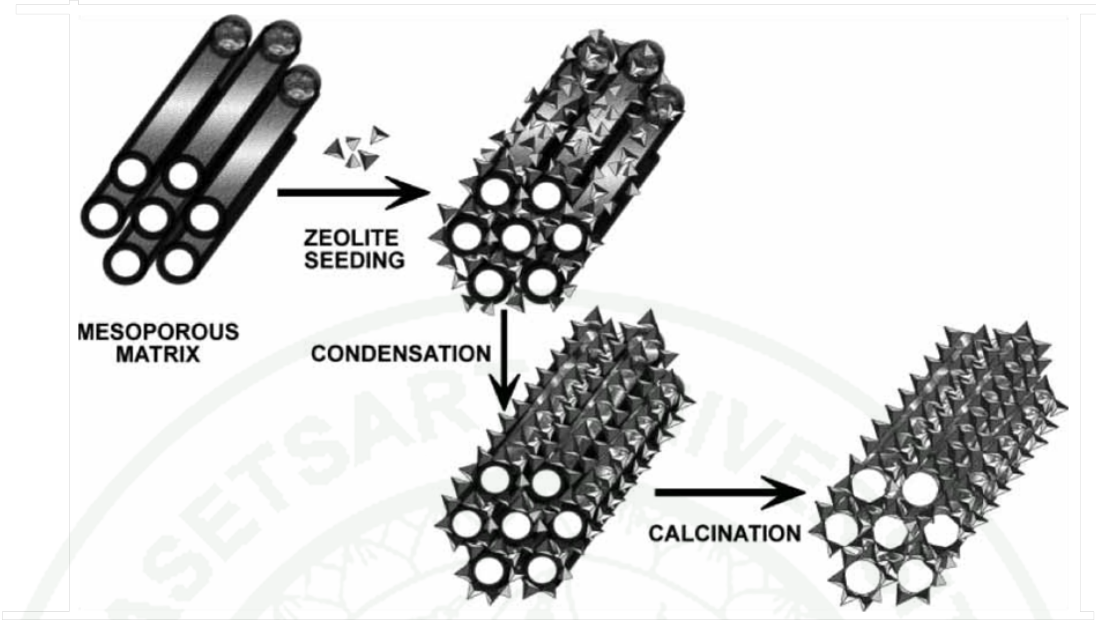

Figure 13 Mechanism of self-organization of zeolite seeds onto mesoporous matrix.

Source: Čejka and Mintova, (2007)

In this work, ZSM-5–SBA-15 composites was prepared following the supramolecular templating method. ZSM-5 zeolite prepared from 4-18 h hydrothermal treatment time periods was used as zeolite seeding, sodium silicate was used as an additional source of silica, and Pluronic P123 was used as supramolecular template for the synthesis of SBA-15 structure. Since the synthesis condition of ZSM-5 zeolite and SBA-15 mesoporous silica were extremely different, only few reports demonstrating the ZSM-5–SBA-15 composites formation. Therefore, it was a great challenge to apply the Ni/ZSM-5–SBA-15 catalyst that provided the significant characteristics of pore structure as the catalyst for CO_2 hydrogenation with CH_4 process. The detail of catalytic performance test was shown in the next section.

MATERIALS AND METHODS

In this chapter, the information including the materials and equipment, and the experimental preparation and procedure regarding ZSM-5–SBA-15 composite material were described. In the first part, chemicals and characterization devices used in the preparation of support and catalyst, testing units of catalytic dry reforming performances and product analysis unit were explained. The methods of catalyst synthesis and catalyst performance testing including the preparation of zeolite, silica and zeolite/silica composites support, metal loading techniques were reported in the second part and the investigation of CO_2 hydrogenation with CH_4 reaction were explained in detail.

Materials and equipment

The materials and chemicals used for ZSM-5 zeolite, SBA-15 mesoporous silica and ZSM-5–SBA-15 composites supports preparation; Ni/ZSM-5, Ni/SBA-15 and Ni/ZSM-5–SBA-15 composites catalyst preparation; and performances of CO_2 hydrogenation with CH_4 reaction were listed below.

1. Materials and equipment for support preparation

Materials

1. Sodium silicate solution (NaO_3Si, 32 wt% SiO_2, PQ Corporation)
2. Aluminium nitrate ($Al(NO_3)_3 \cdot 9H_2O$, 98.0% purity, UNILAB)
3. Hydrochloric acid (HCl, 36.5-38.0 wt% purity, J.T. Baker)
4. Tetrapropyl ammonium bromide (TPABr) ($C_{12}H_{28}BrN$, 98.0% purity, Fluka)
5. Distilled water

Equipment

1. Glassware
2. Digital balance (AT 400, Metler Toledo)
3. Digital hot plate and stirrer (SLR, Schott)
4. pH meter (CG842, Schott)
5. Mortar & pestle (P/N 161-5035, 35 mm, PIKE technologies)
6. Heating oven (ED53, Binder)
7. Laboratory chamber furnaces (CFW 1300, Carbolite)
8. Autoclave (In-house fabrication) was used in the stage of hydrothermal treatment process in catalyst preparation. The elevated temperature and pressured were used in processing materials (Figure 14).

Figure 14 Teflon-lined pressurized device designed for hydrothermal aging process.

9. Ultrasonic bath (AK-150, ACME-KORN)
10. Desiccator (Schott)

Characterization equipment

1. Crystal phase analysis (Powder X-ray diffraction spectroscopy (XRD)) (Phillips X'pert IMS, Cu-α radiation)

2. Surface area and pore size analysis (N_2 adsorption Analysis) (Quantachrome Corporation, Autosorb-1C)

3. Structure analysis (Scanning electron microscopy (SEM)) (JEOL, JSM-6301) and (Transmission electron microscopy (TEM)) (JEOL, JEM-2010)

2. Materials and equipment for catalyst preparation

Materials

1. Nickel nitrate ($Ni(NO_3)_2 \cdot 6H_2O$, 97.0% purity, UNILAB)
2. Tetrahydrofuran (THF, C_4H_8O, UNILAB)
3. Distilled water

Equipment

1. Glassware
2. Digital balance (AT 400, Metler Toledo)
3. Digital hot plate and stirrer (SLR, Schott)
4. Oven (ED53, Binder)
5. Laboratory chamber furnaces (CFW 1300, Carbolite)
6. Desiccator (Schott)

3. Materials and equipment for CO_2 hydrogenation with CH_4 performance test

Materials

1. Feed gases

   1.1 Methane (CH_4, 99.99 % purity, TIG)
   1.2 Carbon dioxide (CO_2, 99.5 % purity, SCE)
   1.3 Hydrogen (H_2, 99.99 % purity, TIG)
   1.4 Nitrogen (N_2, 99.99 % purity, TIG)

2. Standard gases

   2.1 Mixture of 36% carbon monoxide (CO) and 64% hydrogen, TIG.
   2.2 Mixture of 25% carbon monoxide (CO), 25% carbon dioxide (CO_2), 25% methane (CH_4), in hydrogen (H_2) balance, TSG.

3. Quartz wool as the catalyst bed support (Alltech)

Equipment (Figure 15)

1. Pressure regulator (Harris)
2. Mass flow controller (GFC117 Model, Aalborg) (Figure 16)
3. Mass flow controller (8300 series, KOFLOC)
4. Thermocouple (K type)
5. Temperature controller (120-R/E, Shinho)
6. Temperature indicator (RI, Shinho)
7. Tube furnace (MTF 12/38/250 Model, Carbolite) (Figure 17)
8. Flexible heating tape (100 Volt)
9. Voltage transformer (SB-5, SLIDEUP)
10. Bubble flow meter

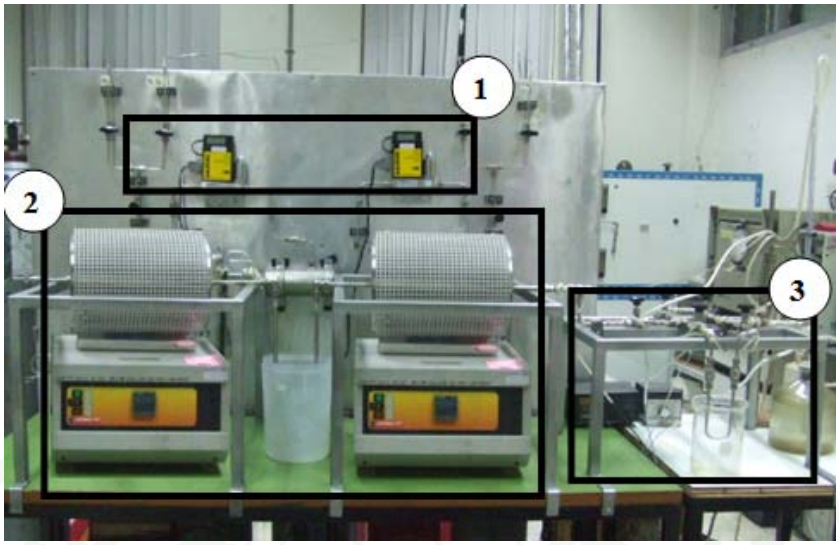

Figure 15 Catalytic reaction testing unit: (1) a feed flow measuring and controlling system, (2) the furnace-equipped inconel alloy tube reactor and, (3) a sampling system.

Figure 16 Mass flow controller (GFC117 Model, Aalborg).

Figure 17 Tube furnace (MTF 12/38/250 Model, Carbolite).

Characterization equipment

1. Gas chromatograph equipped with thermal conductivity detector (TCD)(GC-2014 Model, Shimadzu)

Experimental procedures

In this research, ZSM-5 zeolite, SBA-15 mesoporous silica and ZSM-5–SBA-15 composites supports were prepared before Ni loading and then Ni/ZSM-5, Ni/SBA-15 and Ni/ZSM-5–SBA-15 composites catalysts were tested for CO_2 hydrogenation with CH_4 performance. In details, ZSM-5 zeolite was firstly prepared and characterized, then ZSM-5 zeolite with suitable structure were used as seeding to synthesize ZSM-5–SBA-15 composites. After that, Ni metal was loaded on ZSM-5, SBA-15 and ZSM-15/SBA-15 composites by impregnation technique before the performance of CO_2 hydrogenation with CH_4 tested.

1. Support preparation

1.1 ZSM-5 zeolite preparation

Sodium silicate and aluminium nitrate were used as reactants. TPABr template was used as the structure-directing agent. The SiO_2: Al_2O_3: TPABr: H_2O molar composition of the resulting gel was 1: 0.05: 0.03: 60. The detailed procedures were as follows:

1.1.1 A solution of TPABr surfactant was prepared by adding 0.371 g of TPABr in 40 mL distilled water at room temperature and then it was stirred until the clear solution was obtained.

1.1.2 Sodium silicate solution and aluminium nitrate solution were added into the TPABr solution drop by drop at constant pH (pH 10.5) under vigorous stirring. Then, the mixed solution was kept stirring for 30 minutes at room temperature.

1.1.3 The resulting gel was transferred to a Teflon-lined autoclave and isothermally heated at 240 °C for 4-18 h under autogeneous pressure.

1.1.4 The solid product was washed with large amounts of warm distilled water and separated by mean of filtration.

1.1.5 The solid product was dried at 80 °C for 12 h. Then, some amount of dried product was separated and calcined at 600 °C for 5 h before characterization. All steps were summarized as shown in Figure 18.

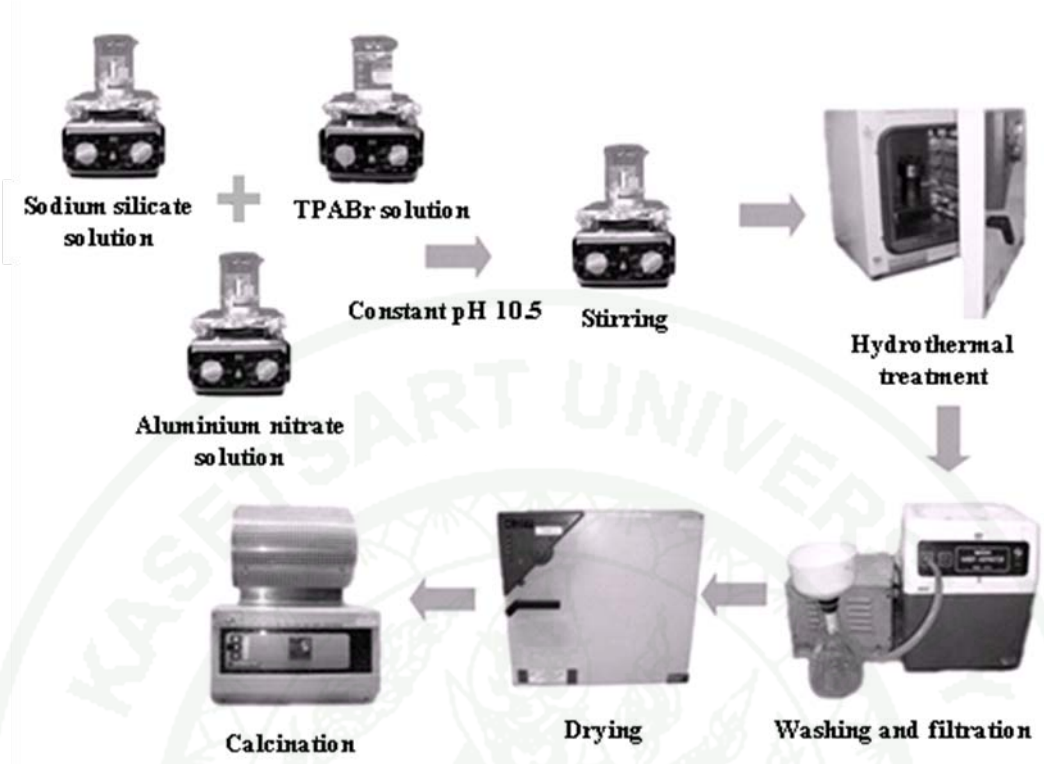

Figure 18 Scheme of ZSM-5 zeolite synthesis process.

1.2 SBA-15 mesoporous silica preparation

The equipment set up in this experiment was shown in Figure 19.

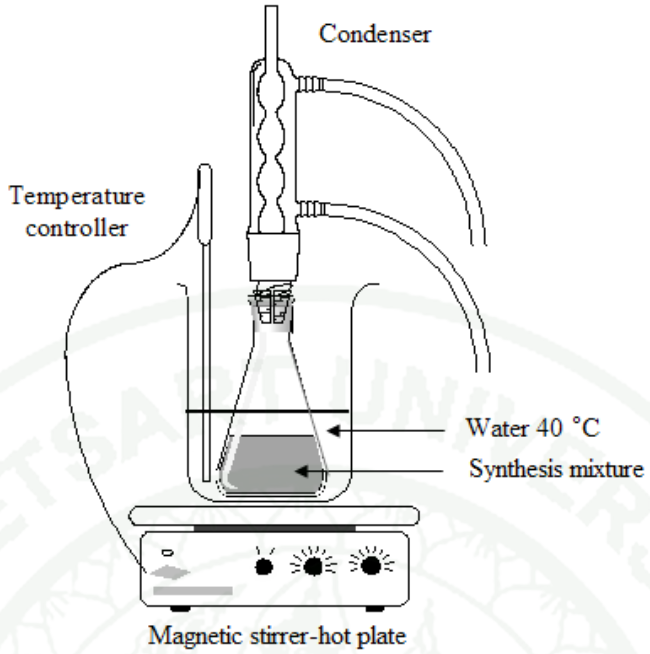

Figure 19 The equipment setup of hydrolysis - condensation process.

1.2.1 A solution of surfactant was prepared by stirring 0.00875 mol (0.845 g) Pluronic P123 in 60 mL distilled water at room temperature until the clear solution was obtained.

1.2.2 Sodium silicate solution (based on 1 g of silica) prepared from was added to Pluronic P123 solution and mixed properly.

1.2.3 After that, 4 mol of HCl solution (5.4 mL) was quickly added into the mixture under vigorous stirring at 40 °C and the obtained mixture was stirred for 24 h. From this stage, the gel product was prepared.

1.2.4 The resulting gel was transferred to a Teflon-lined autoclave and isothermally heated at 100 °C under autogeneous pressure for 24 h.

1.2.5 The solid product was washed with large amounts of warm distilled water and separated by mean of filtration.

1.2.6 The solid product was dried at 140 °C for 3 h and then calcined at 600 °C for 5 h to remove an organic template and volatile impurity. All steps were summarized as shown in Figure 20.

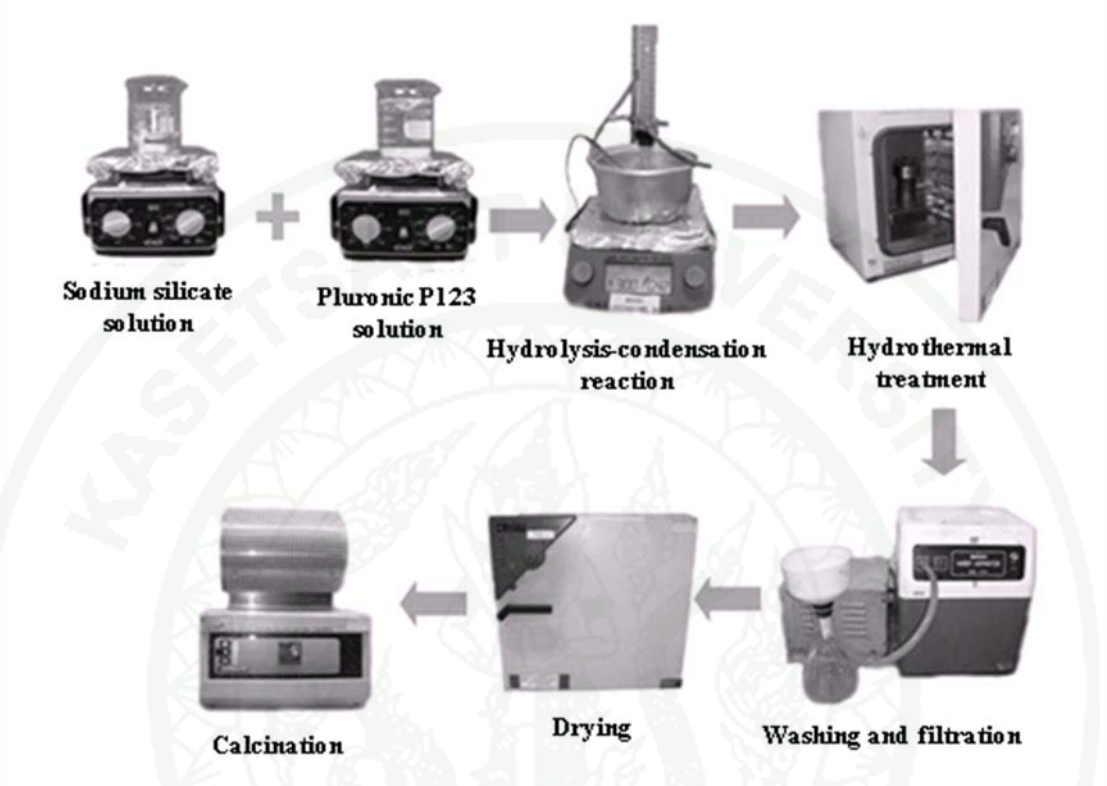

Figure 20 Scheme of SBA-15 mesoporous silica synthesis process.

1.3 ZSM-5–SBA-15 composites preparation

In this series of experiment, ZSM-5–SBA-15 composites was synthesized using ZSM-5 zeolite as the seeding and sodium silicate as the silica source. The detailed procedures were as follows:

1.3.1 *Preliminary study*

1.3.1.1 A solution of surfactant was prepared by stirring 0.00875 mol (0.845 g) Pluronic P123 in 60 mL distilled water at room temperature until the clear solution was obtained.

1.3.1.2 ZSM-5 zeolite with 4 h of hydrothermal treatment time periods was added into the solution of surfactant and kept stirring for 30 minutes.

1.3.1.3 Sodium silicate solution (based on 1 g of silica) was added to the mixture.

1.3.1.4 After that, 4 mol HCl solution (5.4 mL) was quickly added into the mixture under vigorous stirring at 40 °C and the obtained mixture was stirred for 24 h. From this stage, the gel product was prepared.

1.3.1.5 The resulting gel was transferred to a Teflon-lined autoclave and isothermally heated at 100 °C under autogeneous pressure for 24 h.

1.3.1.6 The solid product was washed with large amounts of warm distilled water and separated by mean of filtration.

1.3.1.7 The solid product was dried at 140 °C for 3 h and then calcined at 600 °C for 5 h to remove the organic template and volatile impurity.

1.3.2 *Effect of Pluronic P123 on the structure of ZSM-5 zeolite*

The 12 h of hydrothermal treatment time periods ZSM-5 zeolite was selected to use as seeding. The details of synthesis step were same as 1.3.1 but without sodium silicate adding (step 1.3.1.3).

1.3.3 *Effect of adding sequence study*

In this section, the synthesis order was separated into 2 pathways depended on the adding sequence. The detailed procedures were as follows:

1.3.3.1 ZSM-5 + Sodium silicate + HCl + Pluronic P123 (HCl-P123)

1) ZSM-5 zeolite was added into sodium silicate solution (based on 1 g of silica) and 30 mL DI water. The mixture was kept stirring for 30 minutes.

2) Then, 4 mol HCl solution (5.4 mL) were added into the mixed solution and kept stirring for another 1 h.

3) After that, the solution of surfactant Pluronic P123 and 30 mL distilled water were added into the mixed solution under vigorous stirring at 40^{o}C and the obtained mixture was stirred for 24 h. From this stage of experiment, the gel product was prepared.

4) The resulting gel was transferred to a Teflon-lined autoclave and isothermally heated at 100 °C for 24 h under autogeneous pressure.

5) The solid product was washed with large amounts of warm distilled water and separated by mean of filtration.

6) The solid product was dried at 140 °C for 3 h and then calcined at 600 °C for 5 h to remove the organic template and volatile impurity.

1.3.3.2 ZSM-5 + Sodium silicate + Pluronic P123 + HCl (P123-HCl)

1) ZSM-5 zeolite was added into sodium silicate solution (based on 1 g of silica) and 30 mL DI water. The mixture was kept stirring for 30 minutes.

2) The solution of surfactant Pluronic P123 and 30 mL distilled water were added into the mixed solution and kept stirring for another 1 h.

3) After that, the 4 mol HCl solution (5.4 mL) was added into the mixed solution under vigorous stirring at 40 °C and the obtained mixture was stirred for 24 h. From this stage of experiment the gel product was prepared.

4) The resulting gel was transferred to a Teflon-lined autoclave and isothermally heated at 100 °C for 24 h under autogeneous pressure.

5) The solid product was washed with large amounts of warm distilled water and separated by mean of filtration.

6) The solid product was dried at 140 °C for 3 h and then calcined at 600 °C for 5 h to remove the organic template and volatile impurity.

1.3.4 *Effect of ZSM-5 zeolite particle size on composite structure*

The seeding ZSM-5 zeolite was changed into 7 h of hydrothermal treatment time periods in order to reduce particle size of ZSM-5 zeolite seeding. The synthesis conditions were compared between 3 methods. The detailed procedures were as follow.

1.3.4.1 ZSM-5 (7 h) + P123-HCl

Similar techniques as mentioned in 1.3.3.2 were applied

1.3.4.2 Ground ZSM-5 (7 h)+ P123-HCl

1) ZSM-5 zeolite was ground into the smaller size before used.

2) Similar techniques as mentioned in 1.3.3.2 were applied

1.3.4.3 Ground ZSM-5 (7 h)+ P123-HCl(UT)

1) ZSM-5 zeolite was ground into the smaller size before used.

2) ZSM-5 zeolite was added into sodium silicate solution (based on 1 g of silica) and 30 mL DI water. The mixture was sonicated in ultrasonic bath for 30 minutes.

3) The solution of surfactant Pluronic P123 and 30 mL distilled water were added into the mixed solution and kept sonicating for another 1 h.

4) After that, the 4 mol HCl solution (5.4 mL) was added into the mixed solution under sonicating at 40 °C and the obtained mixture was sonicated for 4 h. From this stage of experiment the gel product was prepared.

5) The resulting gel was transferred to a Teflon-lined autoclave and isothermally heated at 100 °C for 24 h under autogeneous pressure.

6) The solid product was washed with large amounts of warm distilled water and separated by mean of filtration.

7) The solid product was dried at 140 °C for 3 h and then calcined at 600 °C for 5 h to remove the organic template and volatile impurity.

2. Catalyst loading

In this section, Ni-based catalysts (based on 5 wt% nickel loading) were prepared by wet impregnation method. ZSM-5 zeolite, SBA-15 mesoporous silica and ZSM-5–SBA-15 composites prepared by the process mentioned previously were used as the supports in this series of experiment. The procedure of catalyst preparation was explained below:

2.1 The solution of metal precursor was prepared by dissolving 0.26 g of nickel nitrate ($Ni(NO_3)_2 \cdot 6H_2O$) in distilled water.

2.2 The nickel nitrate solution was slowly added into 1 g of supports, and then vigorously stirred at room temperature until sample paste was obtained (Figure 21).

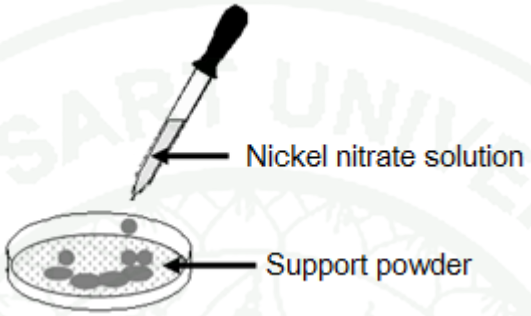

Figure 21 The stage of metal loading in wet impregnation methods.

2.3 The solid product was dried at 100 °C for 3 h and then calcined at 550 °C for 6 h.

3. The performance of catalysts in CO_2 hydrogenation with CH_4

Before testing the catalytic performance, 0.1 g of Ni/ZSM-5, Ni/SBA-15 and Ni/ZSM-5–SBA-15 catalysts were mixed with 0.4 g of sand and packed in an inconel alloy tube reactor. The reactor was placed horizontally in the center of a tubular furnace equipped with a K-type thermocouple located in the center of the catalyst bed. Prior to each experiment, the catalyst was activated by reduction in H_2 atmosphere at 700 °C for 12 h.

During the reaction, CO_2 and CH_4 were converted to synthesis gas in the presence of nickel catalysts at the temperature ranges of 550-650°C with the CO_2/CH_4 molar ratio of 1, total gas pressure of 1 bar and gas hourly space velocity (GHSV) of 8,400–24,000 mL h^{-1} g_{cat}^{-1}. The effluent gases are analyzed by gas chromatography (GC) equipped with thermal conductivity detector (TCD, GC-2014, Shimadzu) at the condition as shown below.

- Initial carrier gas (He) flow rate	25	mL/min
- Injector temperature	100	^{o}C
- Initial column temperature	100	^{o}C
- Final column temperature	100	^{o}C
- Detector temperature	150	^{o}C
- Current	100	mA

The details of qualitative and quantitative analysis results from gas chromatographs are reported in Appendix A. The data of CH_4 and CO_2 conversions and H_2 and CO yields calculated from gas chromatographs results and the detail of calculation are shown in Appendix B.

RESULTS AND DISCUSSION

In this present research, ZSM-5–SBA-15 composites with micro/mesoporous structure were synthesized from ZSM-5 zeolite by modified SBA-15 synthesis process using sodium silicate as an additional silica source. ZSM-5–SBA-15 composites sample of uniform structure was selected for Ni metal loading (based on 5 wt% nickel) in order to investigate performances of CO_2 hydrogenation with CH_4 compared to those of Ni/SBA-15 and Ni/ZSM-5 catalysts. The reaction conditions used in this stage were as follows: CO_2/CH_4 molar ratio, 1; temperature, 500-650 ºC; total pressure, 1 atm; and GHSV, 8,400-24,000 mL h^{-1} g_{cat}^{-1}.

1. Physical properties and morphologies of supports

1.1 ZSM-5 zeolite

ZSM-5 zeolite was prepared following the synthesis method reported by Chareonpanich *et al.* (2004) and the hydrothermal treatment time periods were varied in the range of 4-18 h. The particle size and crystal structure of ZSM-5 zeolite were examined by XRD and SEM techniques before the use as precursor to prepare ZSM-5–SBA-15 composites. The XRD result shown in Figure 22 confirmed the formation and crystallinity of ZSM-5 zeolite. It was found that ZSM-5 zeolite could be hardly formed at the hydrothermal treatment time period of 4 h. The intensity of ZSM-5 zeolite was increased with increasing the hydrothermal treatment time period, indicating the increase of particle size of ZSM-5 zeolite. The same trend was also found in SEM results shown in Figure 23, the larger particle size of ZSM-5 zeolite was obtained and the morphology was changed with the increase of hydrothermal treatment time periods. This result was in agreement with the result reported by Anuwattana *et al.* (2008), indicating significant dependences of the formation, growth and crystallinity of ZSM-5 zeolite on the hydrothermal treatment temperature and time period.

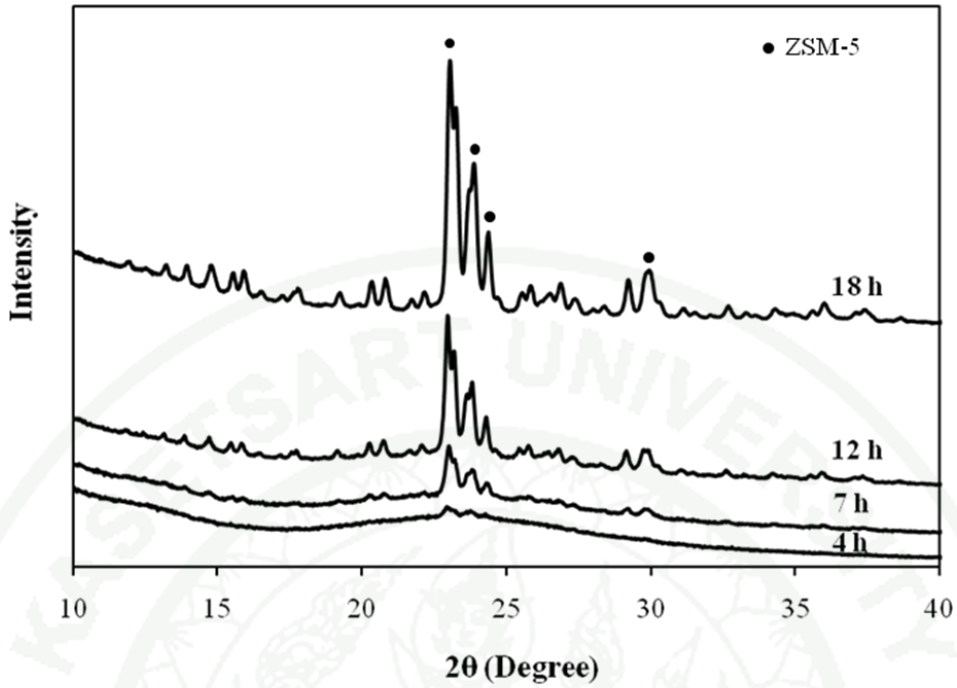

Figure 22 XRD patterns of ZSM-5 zeolites synthesis at the hydrothermal treatment time periods of 4-18 h.

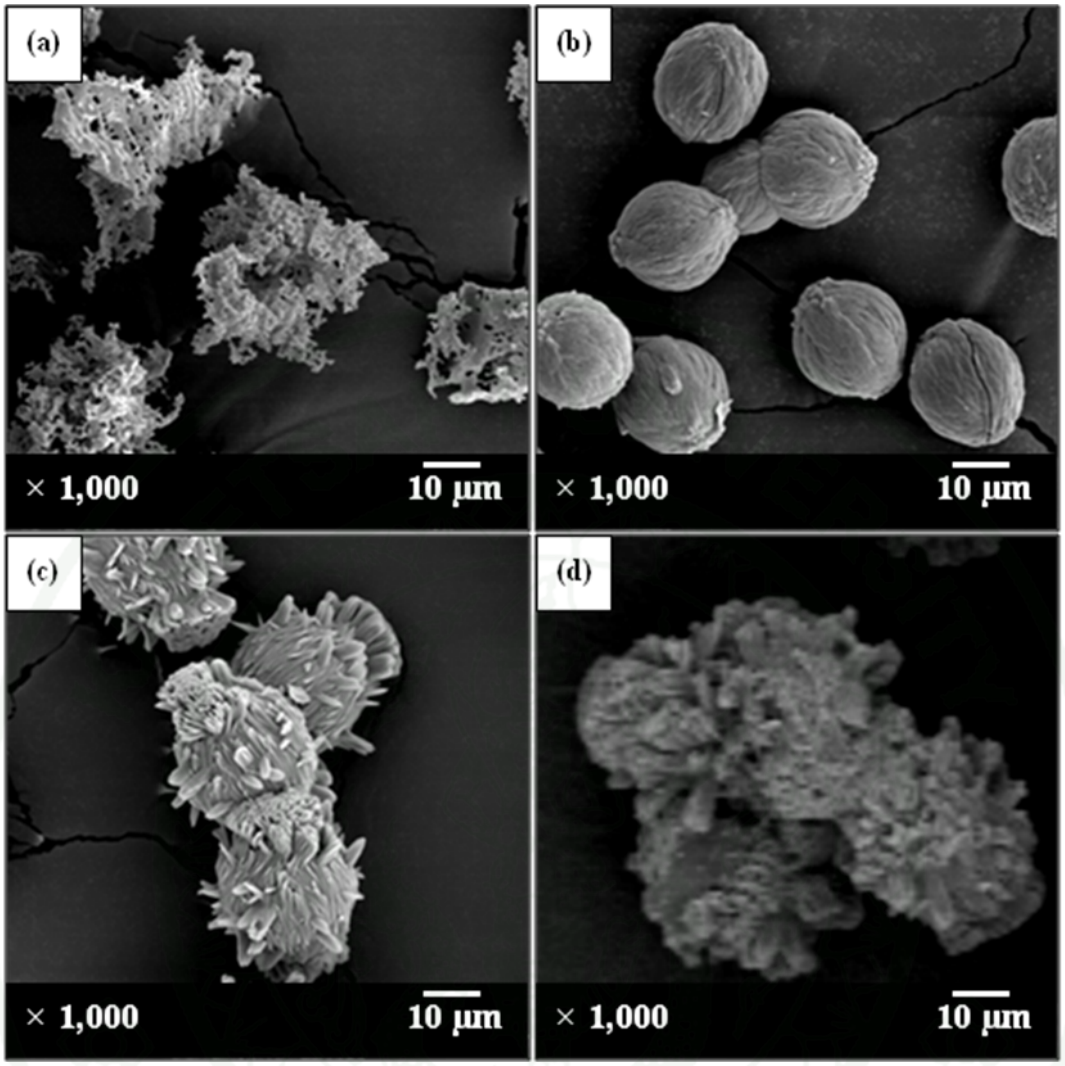

Figure 23 SEM images of ZSM-5 zeolites synthesis at the hydrothermal treatment time periods of (a) 4 h, (b) 7 h, (c) 12 h, and (d) 18 h.

1.2 Ordered SBA-15 mesoporous silica

SBA-15 mesoporous silica was prepared following the synthesis method reported by Zhao *et al.* (1998). The characteristics of SBA-15 were investigated by using N_2 adsorption-desorption isotherm, SEM and TEM techniques as shown in Figures 24 and 25. The type IV isotherm with a hysteresis loop at relative pressure of 0.65 – 0.95 and the pore size of 6.6 nm revealed the existence of mesoporous structure of the sample. For the SEM and TEM images as shown in Figure 25, the angles of view were described. The rod-like structure (side view) was shown in the SEM image

in Figure 25(a) and the overlap of hexagonal pore structure (front and side views) was clearly shown in TEM image in Figure 25(b) also confirmed the SBA-15 characteristics of the sample.

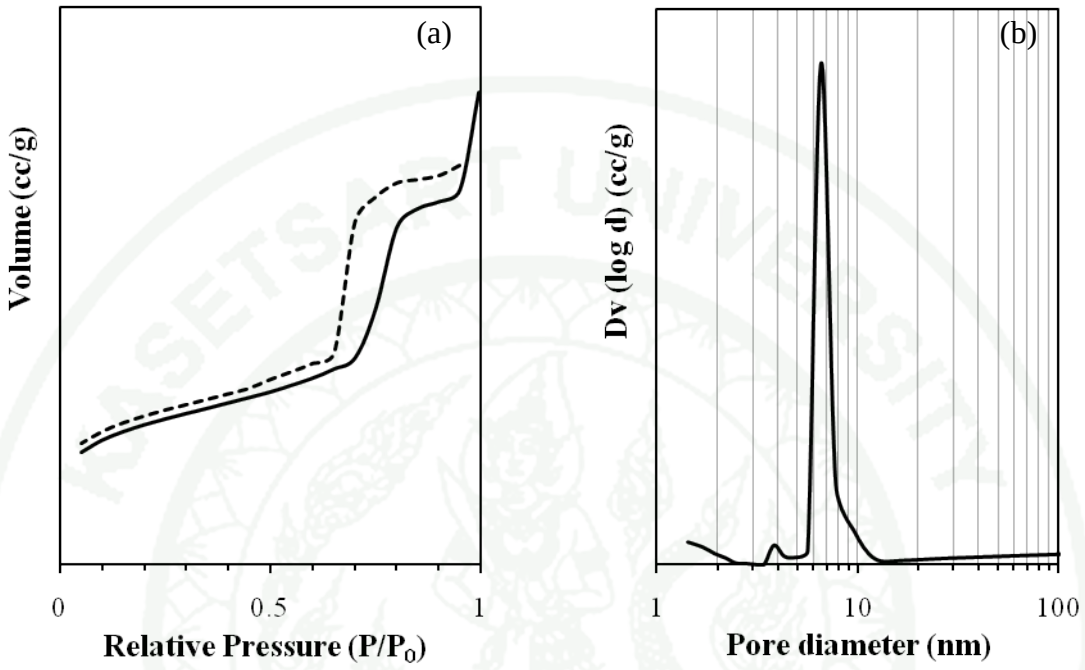

Figure 24 (a) N_2 sorption isotherm and (b) BJH pore size distribution (desorption) of SBA-15 mesoporous silica.

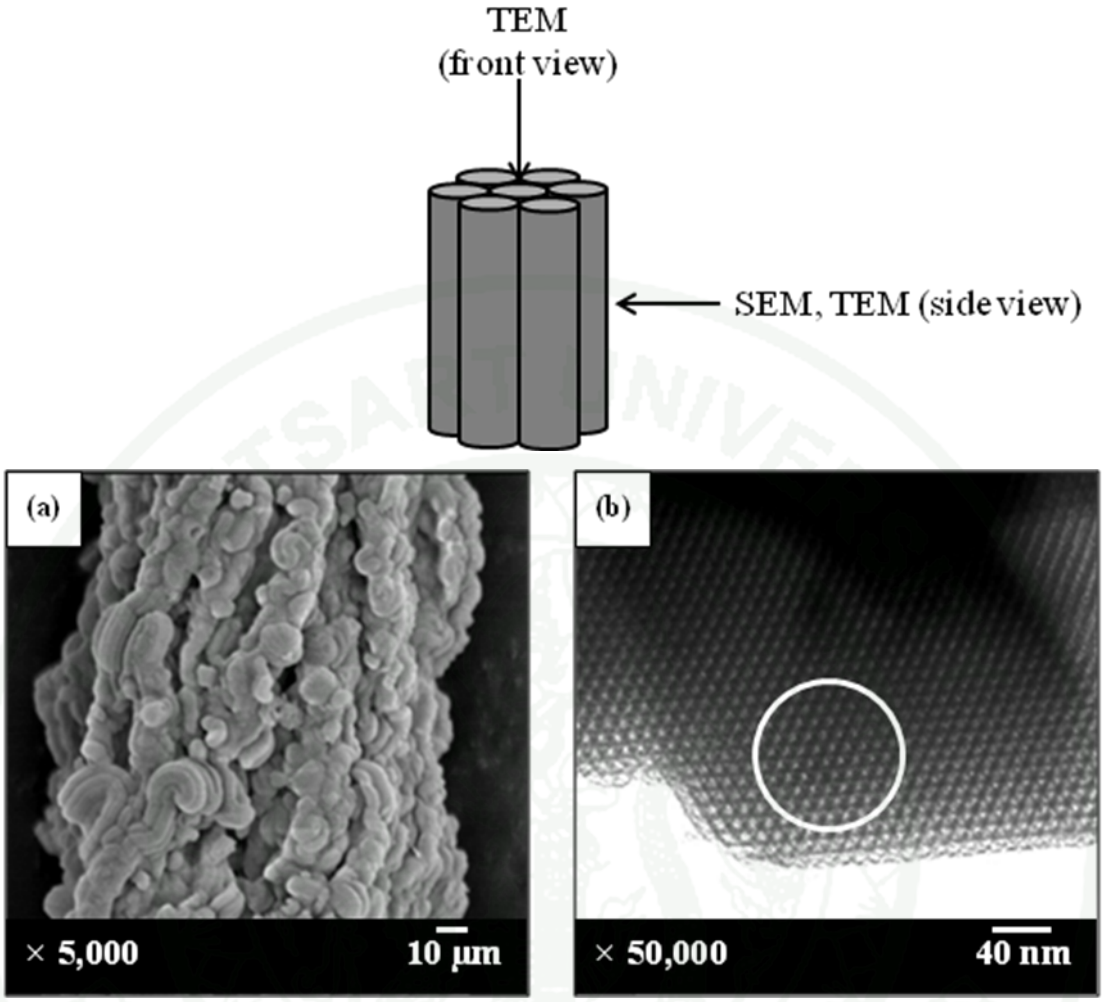

Figure 25 View angles of (a) SEM (side view) and (b) TEM (front and side views) images of SBA-15 mesoporous silica.

1.3 ZSM-5–SBA-15 composites

After ZSM-5 zeolite was successfully synthesized, it was used as the seeding to synthesize ZSM-5–SBA-15 composites using the modified SBA-15 synthesis process. The effect of amount of ZSM-5 seeding was investigated in the preliminary study using XRD, N_2 sorption, SEM and TEM techniques. Moreover, the effect of Pluronic P123, the adding sequence and the effect of ZSM-5 hydrothermal treatment time periods on the structure of ZSM-5–SBA-15 composites were also investigated as well.

1.3.1 *Preliminary study – Effect of zeolite content*

In the preliminary study of ZSM-5–SBA-15 composites synthesis, the powder of 4-h hydrothermal treated ZSM-5 zeolite was selected to use as the seeding due to its smallest particle size. The ratios of ZSM-5 zeolite seeding and silica used in synthesis process were varied in the range of 0.5:3 to 2:3 as shown in Table 5.

Table 5 The ratio of 4-h hydrothermal treated ZSM-5:silica in reactant compositions

Sample	ZSM-5: Silica
Z0.5S3	0.5:3
Z1S3	1:3
Z2S3	2:3

The crystallographic structure of the all ZSM-5–SBA-15 composites samples were investigated by XRD, N_2 adsorption-desorption isotherm and TEM as shown in Figures 26-28. The XRD patterns in Figure. 26 showed the increase of ZSM-5 intensity with increasing the ZSM-5 content of the sample. This due to the fact that SBA-15 structure is only detected in the low angle XRD ($2\theta<10°$) and it is detected as amorphous phase in the wide angle XRD ($2\theta>10°$) (Zhao *et al.*, 1998). Moreover, the composites samples were the combination of ZSM-5 zeolite and SBA-15. Therefore, the increase of ZSM-5:silica ratio in the sample increased the ZSM-5 intensity as the result of increasing the ZSM-5 portion.

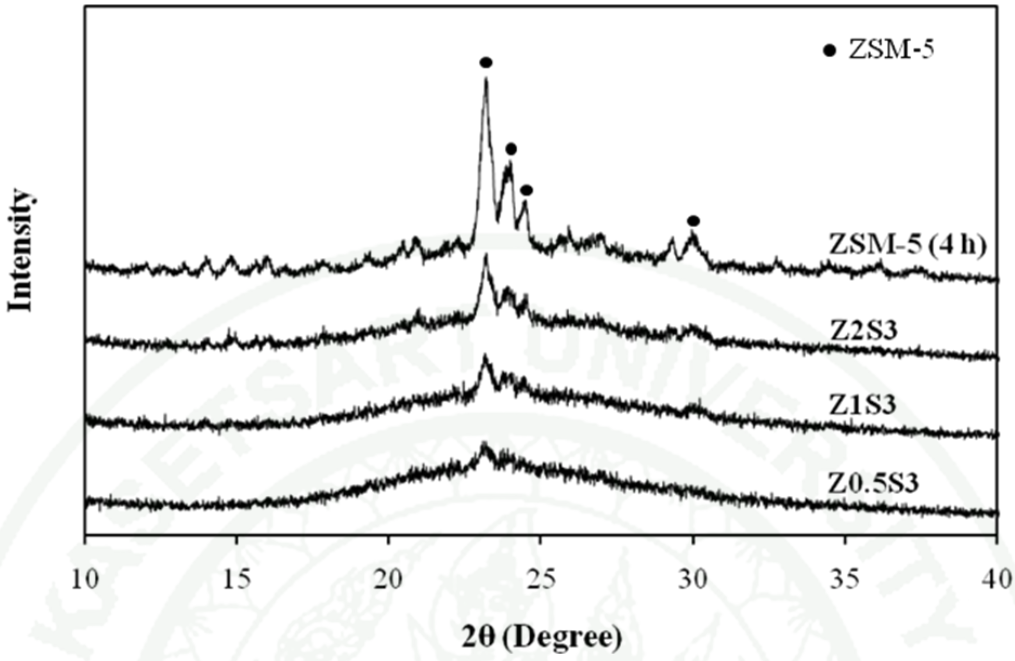

Figure 26 XRD pattern of ZSM-5–SBA-15 composites samples prepared from various ZSM-5:silica ratio in section 1.3.1.

From the N_2 adsorption-desorption isotherm shown in Figure 27, the type I and type IV isotherm with a hysteresis loop at relative pressure of 0.65 – 0.95 revealed the existence of microporous and mesoporous structure of the sample, respectively. In the micro and mesopore size distribution (PSDs) from Figures 28(a) and 28(b), ZSM-5 zeolite and SBA-15 mesoporous silica pore characteristics of the samples were confirmed by the pore size of 5.5 Å and 6.6 nm, respectively.

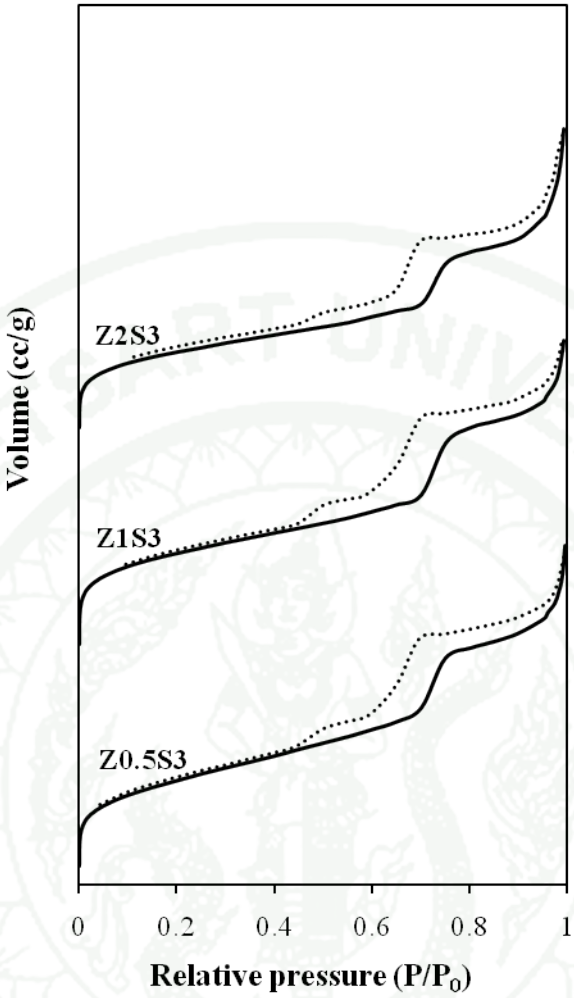

Figure 27 N_2 sorption isotherm of ZSM-5–SBA-15 composites.

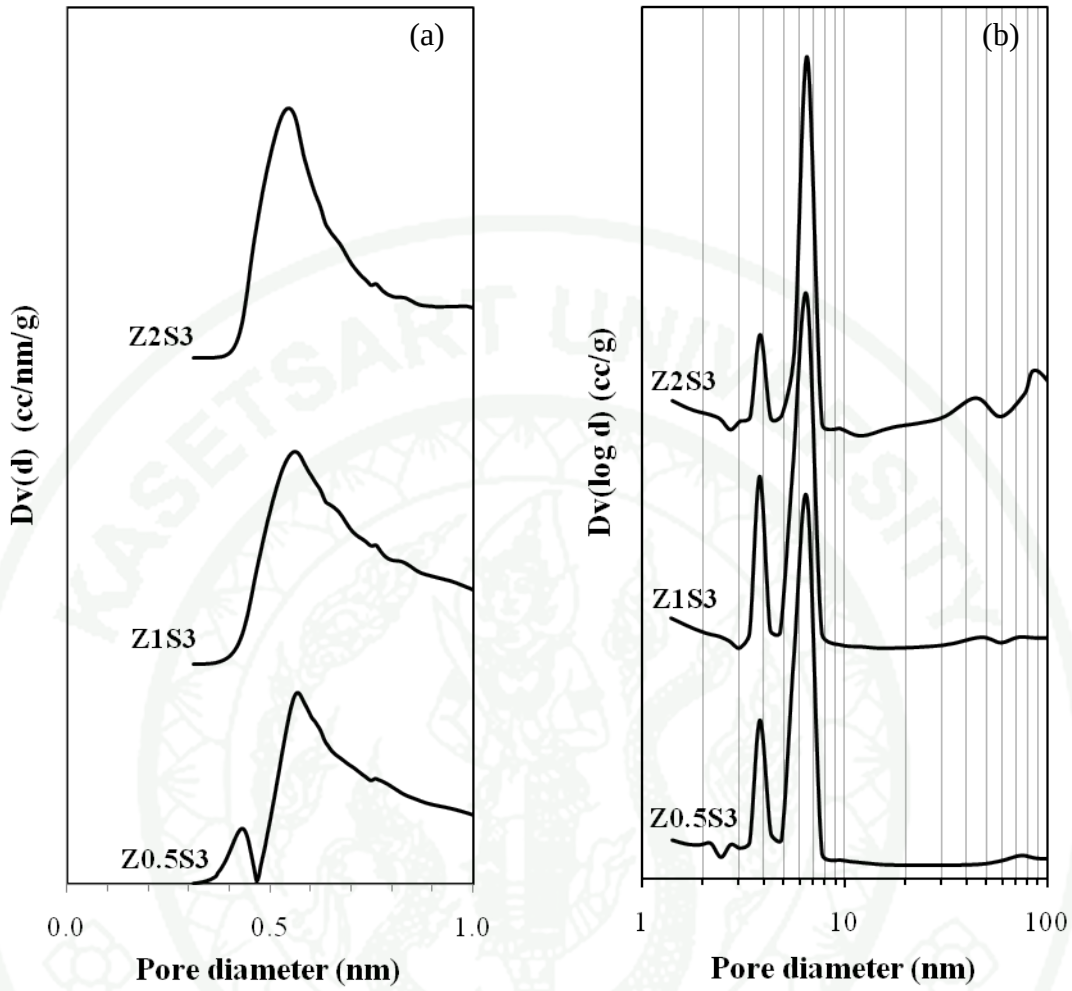

Figure 28 (a) Micro and (b) Meso PSDs of ZSM-5–SBA-15 composites.

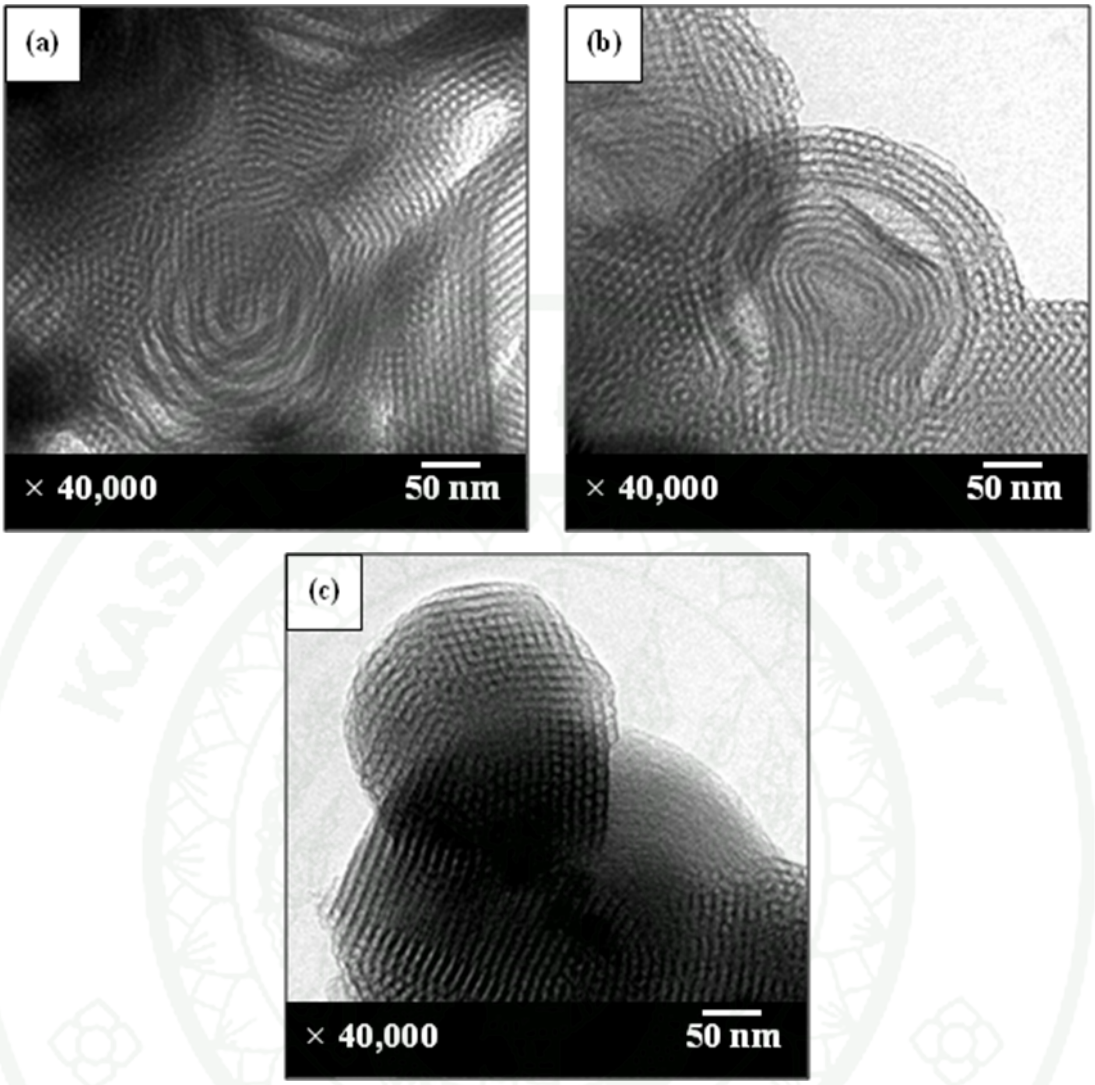

Figure 29 TEM images of (a) Z0.5S3, (b) Z1S3 and (c) Z2S3.

The structural characteristic of ZSM-5 zeolite was clearly confirmed by XRD and N_2 sorption techniques; however, it was not detected by TEM technique as shown in Figure 29. Only the hexagonal mesoporous characteristic of SBA-15 was detected in all samples (Z0.5S3-Z2S3). Therefore, the structure of ZSM-5 zeolite seeding should be reconsidered. ZSM-5 zeolites of 4-h and 7-h hydrothermal treatment time periods were then synthesized and investigated compared to the commercial ZSM-5 zeolite using TEM as the result shown in Figure 30. From Figure 30(a), the structure of 4-h hydrothermal treated ZSM-5 zeolite remained amorphous and did not completely form as the crystalline structure. As a result, the existence of ZSM-5 zeolite was unclearly exposed and ZSM-5 phase was hardly identified by

SEM and TEM techniques. Consequently, after increasing the hydrothermal treatment time period to 7 h, the crystalline structure of ZSM-5 zeolite observed by TEM was shown in Figure 30(b). This structure was similar to the crystalline of commercial ZSM-5 (Figure 30(c)). These results implied that the hydrothermal treatment time period of 4 h did not enough for the formation of ZSM-5 zeolite crystalline and ZSM-5 zeolite synthesized of longer hydrothermal treatment time periods (≥7 h) was needed to use as the seeding for ZSM-5–SBA-15 composites synthesis in order to obtain the complete crystalline structure of ZSM-5 zeolite in the composites.

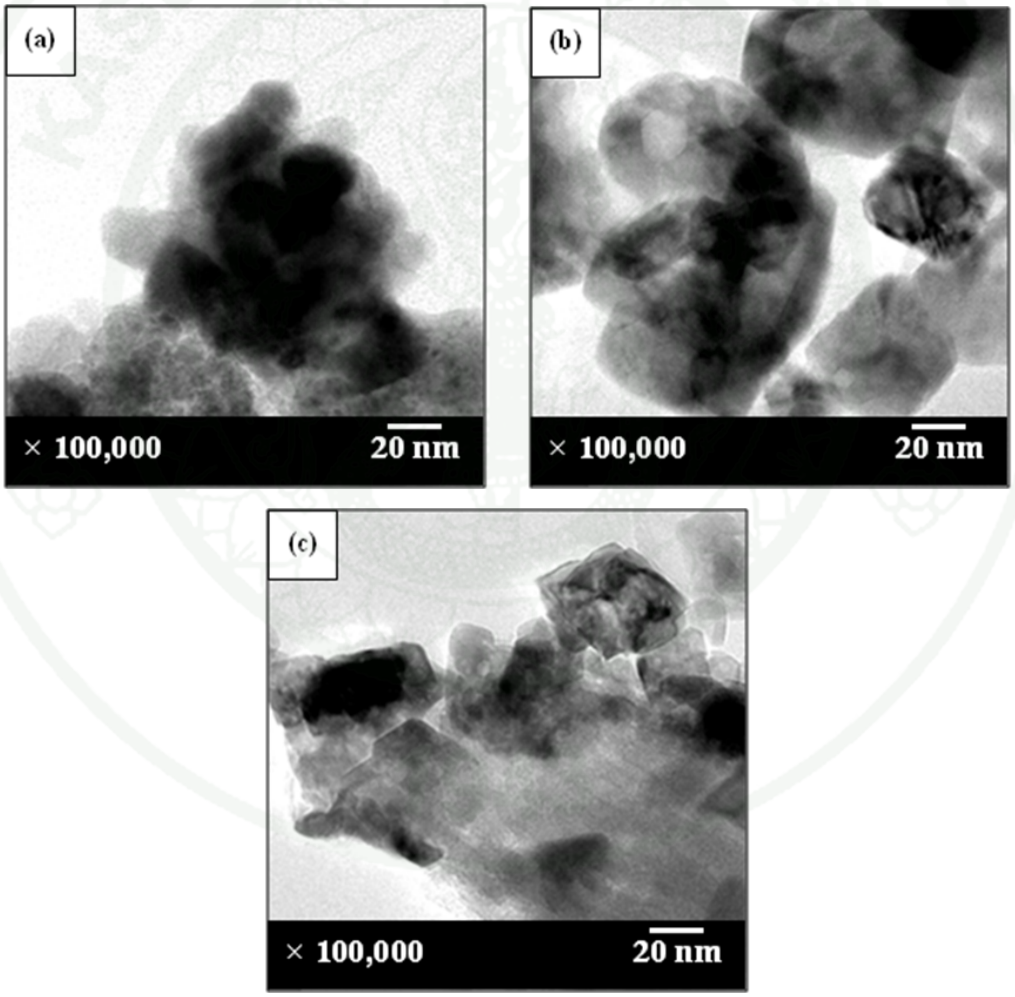

Figure 30 TEM image of (a) 4-h hydrothermal treated (b) 7-h hydrothermal treated and (c) commercial ZSM-5 zeolite.

1.3.2 *Effect of Pluronic P123 on the structure of ZSM-5 zeolite*

The effects of Pluronic P123 and SBA-15 synthesis condition were investigated in order to confirm that the structure of ZSM-5 zeolite could be maintained during the composites was synthesized. The 12-h hydrothermal treated ZSM-5 zeolite was selected to examine the stability of its structure after the composites synthesis without silica adding. The XRD result shown in Figure 31 revealed that the crystal structure of ZSM-5 zeolite remained in the samples. Moreover, the increase of ZSM-5 zeolite intensity was clearly observed. This was due to the fact that the crystalline structure of high-silica zeolite such as ZSM-5 zeolite could resist the high acidic condition and therefore, was not dissolved during the SBA-15 synthesis process (Oudejans, 1984). Meanwhile, the amorphous silica, containing in the ZSM-5 zeolite seeding, was easily dissolved (Liang and Readey, 2005). ZSM-5 portion in the samples was then slightly increased, resulting in the increase of XRD intensity of ZSM-5 zeolite samples.

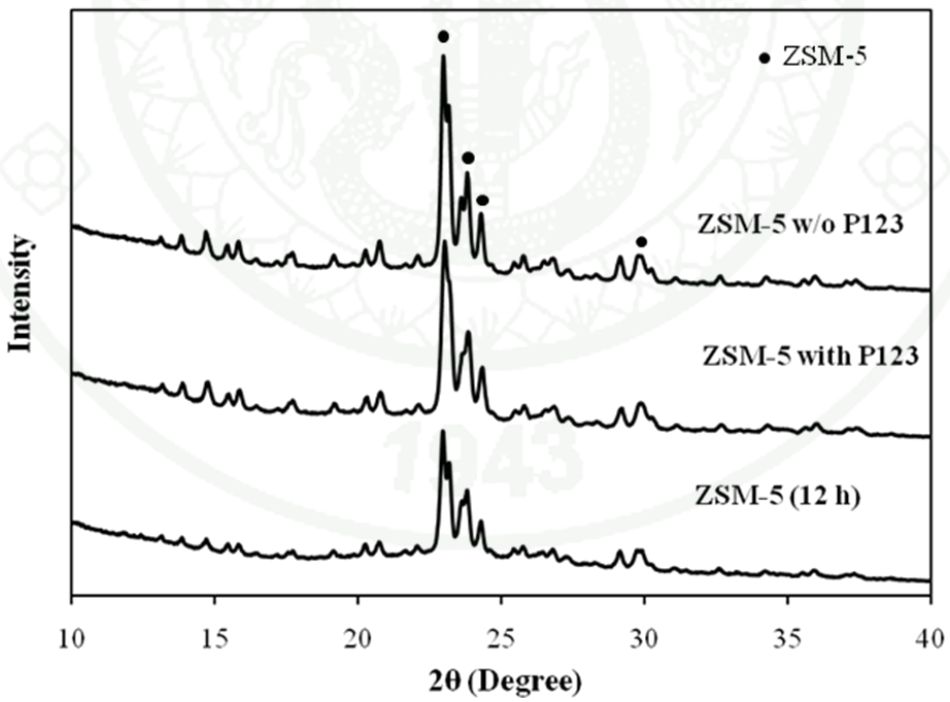

Figure 31 XRD patterns of ZSM-5 (12 h) before and after the composites synthesis with and without Pluronic P123.

The same trend was also found by SEM results shown in Figure 32. Both ZSM-5 zeolites synthesized with Pluronic P123 and without Pluronic P123, the crystalline morphology of ZSM-5 zeolite was still not change. Only amorphous silica was dissolved during composites synthesis stage and it was found that the addition of Pluronic P123 did not affect the ZSM-5 zeolite morphology.

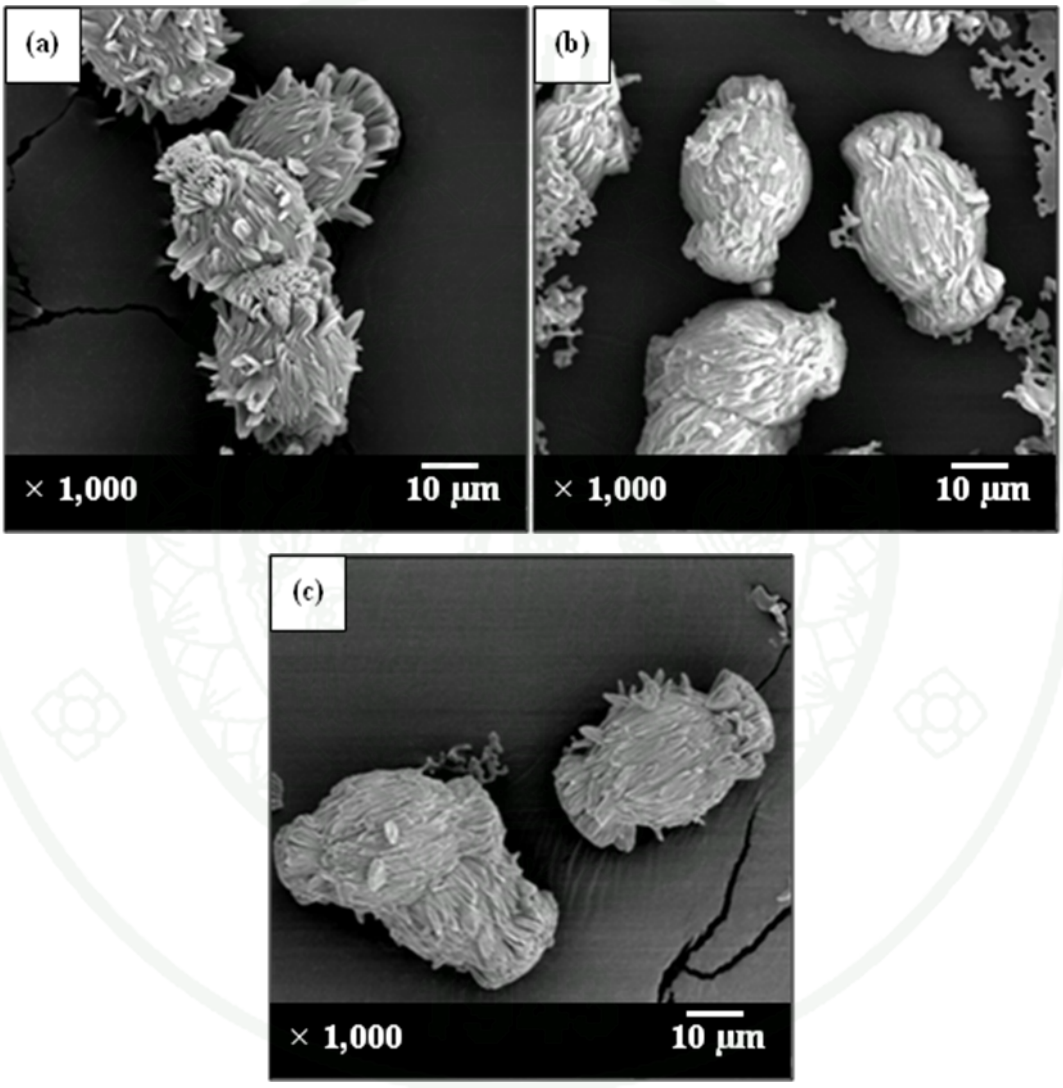

Figure 32 SEM images of (a) ZSM-5 (12 h), (b) ZSM-5 w/o Pluronic P123, and (c) ZSM-5 with Pluronic P123.

1.3.3 *Effect of reactant adding sequence on the structure of ZSM-5–SBA-15 composites*

The reactant adding sequence during ZSM-5–SBA-15 composites synthesis was investigated. In order to clarify the ZSM-5 zeolite phase in the composites, the 18-h hydrothermal treated ZSM-5 zeolite which had the largest particle size among all ZSM-5 zeolite samples was selected to use as the seeding. The adding sequence of sodium silicate (SS), Pluronic P123 solution (P123) and HCl was altered as shown in Table 6. The products were investigated by SEM.

Table 6 The adding sequence in ZSM-5–SBA-15 composites synthesis in section 1.3.3

Sample	Adding sequences
HCl-P123	ZSM-5 (18 h) + Sodium silicate + HCl + Pluronic P123
P123-HCl	ZSM-5 (18 h) + Sodium silicate + Pluronic P123 + HCl

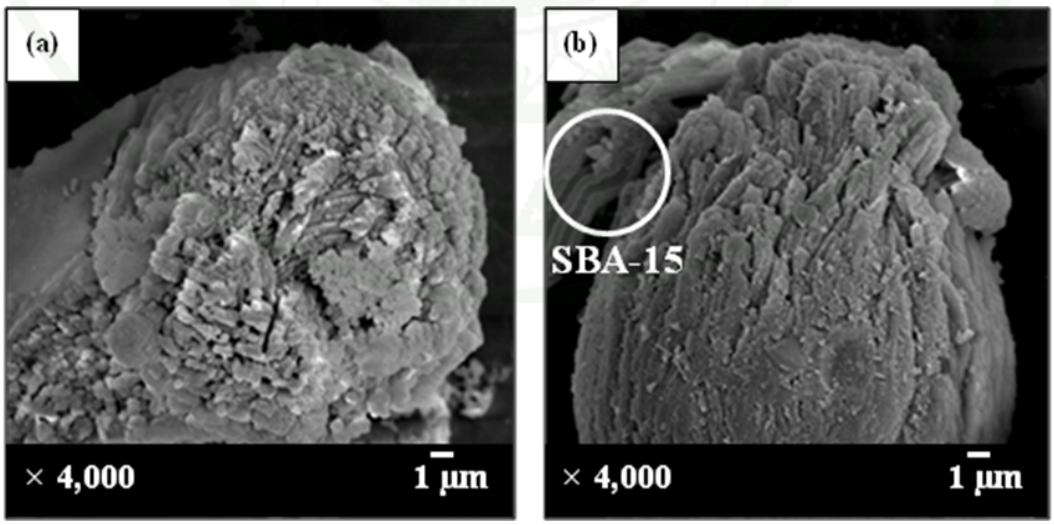

Figure 33 SEM images of (a) HCl-P123 and (b) P123-HCl samples.

From the SEM images of the composites shown in Figure 33, the surface of both HCl-P123 and P123-HCl samples were covered by silica nanoparticles formed during SBA-15 synthesis. SBA-15 structure was only detected in the P123-HCl sample. Similar phenomenon of silica nanoparticles formation was also formed by Zhao *et al.* (1998). The hexagonal structure of SBA-15 was formed by the aggregation of silinol groups on the Pluronic P123 template. For HCl-P123 sample, after HCl acid addition, silinol groups were mainly aggregated among each other and transformed into amorphous silica before the addition of Pluronic P123 template. On the other hand, silinol groups in the P123-HCl sample could easily aggregate with the template before hydrolysis-condensation stage and therefore, led to the formation of SBA-15 mesoporous silica product. However, it was found that the particle size of ZSM-5 zeolite in the P123-HCl sample was too large compared to SBA-15 structure, resulting in the phase separation of ZSM-5 zeolite and SBA-15. Therefore, the smaller size of ZSM-5 particle was needed to incorporate ZSM-5 zeolite into the SBA-15 structure.

1.3.4 *Effect of ZSM-5 zeolite particle size on the ZSM-5–SBA-15 composites structure*

In order to reduce the zeolite particle size, the hydrothermal treatment time period of ZSM-5 zeolite seeding was changed from 18 h to 7 h. The composites synthesis method was modified based on those of section 1.3.3 as shown in Table 7. The sonication technique was applied in the stage of SBA-15 mesoporous silica synthesis following the procedure reported by Chareonpanich *et al.* (2007). The composites samples were investigated by SEM technique as the results shown in Figure 34.

Table 7 The synthesis conditions used in section 1.3.4

Sample	Synthesis conditions
P123-HCl	ZSM-5 (7 h)→ P123-HCl
G-P123-HCl	Ground ZSM-5 (7 h)→ P123-HCl
G-P123-HCl (UT)	Ground ZSM-5 (7 h)→ P123-HCl (Ultrasonic)

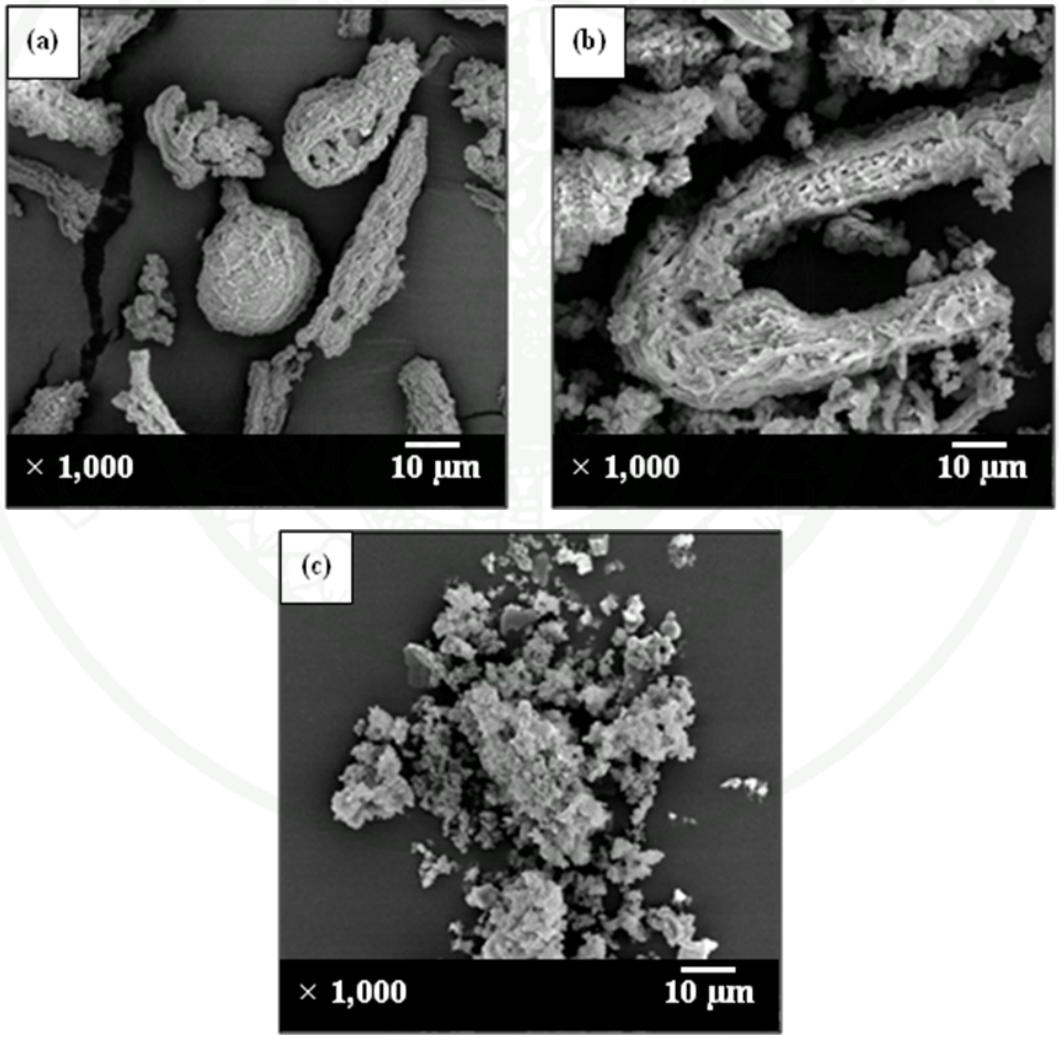

Figure 34 SEM images of (a) P123-HCl, (b) G-P123-HCl and (c) G-P123-HCl (UT) samples.

From SEM image of the composite samples as shown in Figure 34, ZSM-5 zeolites of all samples were encapsulated by SBA-15 mesoporous silica structure. However, the ZSM-5 zeolite structure in the P123-HCl sample was still too large for SBA-15 structure encapsulation (Figure 34(a)). As shown in Figure 34(b), the ground ZSM-5 zeolite structure was much easier encapsulated by SBA-15 because of its smaller size. After the encapsulation/incorporation of ZSM-5 and SBA-15 product was obtained, the synthesis method was then modified using ultrasonic technique in place of magnetic-stirring technique, in order to obtain the product of higher specific surface area and total pore volume within shorter synthesis time (Chareonpanich *et al.*, 2007). From SEM image of G-P123-HCl (UT) sample shown in Figure 34(c), the structure of composites revealed well ZSM-5 zeolite and SBA-15 mesoporous silica incorporation. The structure of G-P123-HCl (UT) composites sample was investigated by TEM and N_2 sorption techniques as shown in Figure 35 and Figures 36-37, respectively.

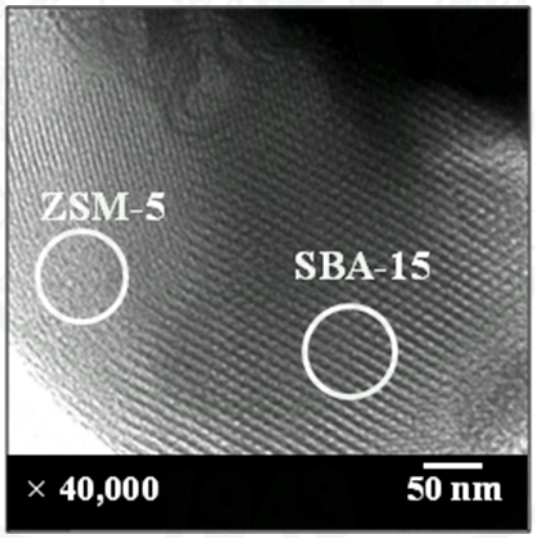

Figure 35 TEM image of G-P123-HCl (UT) samples.

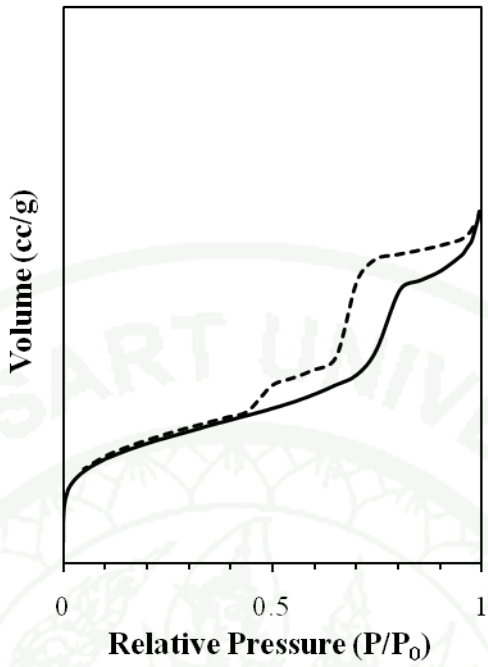

Figure 36 N_2 sorption isotherm of G-P123-HCl (UT) samples.

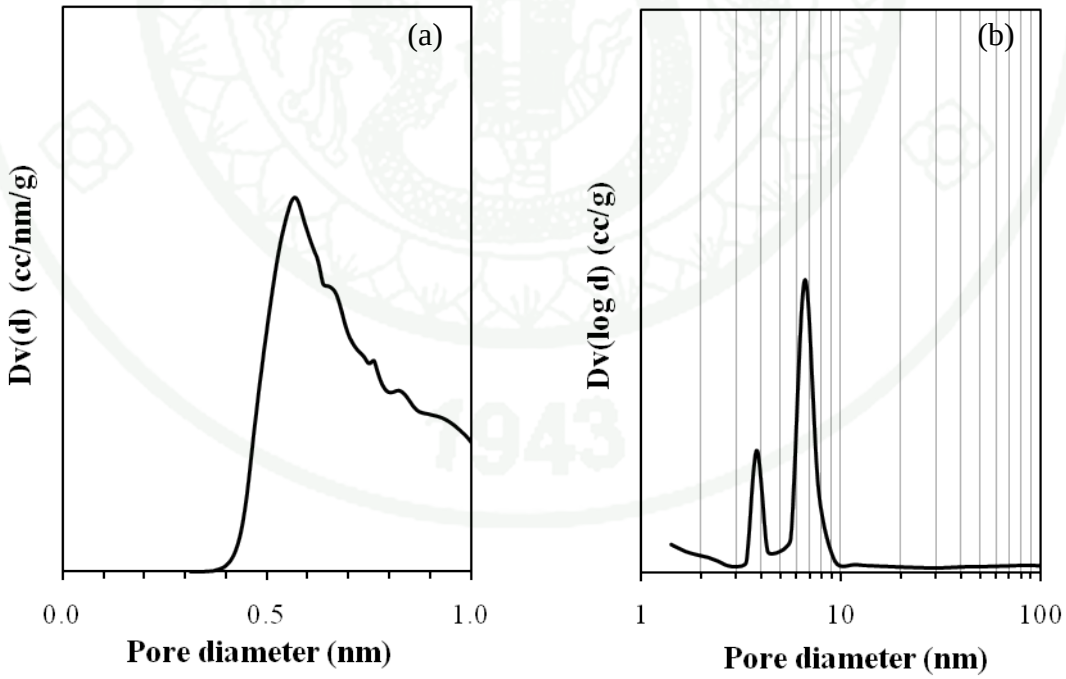

Figure 37 (a) Micro and (b) Meso PSDs of G-P123-HCl (UT) samples.

The TEM images of G-P123-HCl (UT) composites sample in Figure 35 showed the micro and mesoporous structure of approximately 5.5 Å and 6.6 nm, corresponding to ZSM-5 zeolite and SBA-15 porous structures, respectively. From N_2 sorption result, the type I and type IV composite isotherm with hysteresis loop at relative pressure of 0.65 – 0.95, as shown in Figure 36, confirmed the existence of micro and mesoporous structures of composites. Moreover, the pore characteristics of ZSM-5 (5.5 Å) and SBA-15 (6 nm) were also confirmed by micro and mesopore size distributions shown in Figures 37(a) and 37(b). Hence, the composites with the structure of ZSM-5 and SBA-15 was successfully synthesized by using G-P123-HCl (UT) synthesis method and then was used as the composites support for Ni/ZSM-5–SBA-15 catalyst preparation in the next section. The physical properties of all supports used in the next section were investigated by N_2 sorption and the result shown in Table 8

Table 8 Physical properties of supports used in section 2

Support	Specific surface area (m^2/g)	Pore diameter (nm)		Pore volume (cm^3/g)
		micro[a]	meso[b]	
ZSM-5	290	0.55	-	0.16
SBA-15	570	-	6.56	0.92
ZSM-5–SBA-15	505	0.55	6.58	0.69

[a] Calculated by using HK method

[b] Calculated by using BJH desorption method

2. The performance of Ni/ZSM-5–SBA-15 composites catalyst in CO_2 hydrogenation with CH_4

In this series of experiment, the catalyst support, including ZSM-5–SBA-15 composites, ZSM-5 zeolite and SBA-15 mesoporous silica were tested for catalytic performance in CO_2 hydrogenation with CH_4 using nickel as an active metal. Each catalyst was tested in a fixed-bed reactor by using the following operating conditions: CH_4/CO_2 molar ratio of 1, GHSV of 8,400-24,000 $mL \cdot h^{-1}$ g_{cat}^{-1}, the reaction

temperature of 500-650°C and total pressure of 1 atm. The detail data were shown in Appendix Table A2-A4. The conversion and yield results were reported as follows.

2.1 CH_4 and CO_2 conversion

The CH_4 and CO_2 conversion results of Ni/ZSM-5, Ni/SBA-15 and Ni/ZSM-5–SBA-15 catalysts were presented in Tables 9 and 10 as shown below.

Table 9 CH_4 conversion over Ni metal on various catalyst supports

Sample	GHSV ($mL \cdot h^{-1} g_{cat}^{-1}$)	CH_4 conversion			
		500°C	550°C	600°C	650°C
Ni/ZSM-5	24,000	7.0	17.6	23.5	36.2
	18,000	9.2	18.4	28.3	42.7
	12,000	16.2	21.9	36.0	50.2
	8,400	18.8	25.4	39.6	59.0
Ni/SBA-15	24,000	15.7	31.5	45.0	59.4
	18,000	18.0	34.7	50.1	62.8
	12,000	26.7	37.7	53.3	69.4
	8,400	31.6	41.3	57.1	70.8
Ni/ZSM-5–SBA-15	24,000	31.1	48.3	52.3	70.7
	18,000	31.5	48.6	56.3	68.7
	12,000	36.0	51.5	59.9	71.2
	8,400	38.0	53.9	63.0	76.0

Table 10 CO_2 conversion over Ni metal on various catalyst supports

Sample	GHSV ($mL \cdot h^{-1}\ g_{cat}^{-1}$)	CO_2 conversion			
		500°C	550°C	600°C	650°C
Ni/ZSM-5	24,000	7.6	17.2	28.1	42.3
	18,000	9.7	17.7	32.6	47.0
	12,000	6.0	21.4	35.6	51.9
	8,400	8.2	25.6	40.6	56.6
Ni/SBA-15	24,000	19.8	35.8	48.5	67.2
	18,000	21.4	38.3	51.0	69.7
	12,000	19.2	42.2	53.8	70.2
	8,400	25.0	44.2	57.8	68.9
Ni/ZSM-5–SBA-15	24,000	28.8	41.3	55.1	70.9
	18,000	29.4	43.9	56.9	73.7
	12,000	28.6	43.7	56.5	75.7
	8,400	27.9	42.6	55.2	74.9

From the results shown in Tables 9 and 10, it was found that the CH_4 and CO_2 conversions of all catalysts were increased with increasing operating temperature, this was due to the endothermic characteristics of CO_2 hydrogenation with CH_4 reaction (Edwards and Maitra, 1995; Wang *et al*., 1996; Lu and Wang, 1999). Moreover, the decrease of gas hourly space velocity (GHSV) increased the CH_4 and CO_2 conversions, this was due to the increase of reaction times on the catalyst active sites. The poorest CH_4 and CO_2 conversions were obtained by Ni/ZSM-5 catalyst. This result associated with Zhang *et al.* (2005) that due to the fact that the microporous structure of ZSM-5 zeolite support was too small for Ni metal to deposit in the porous structure, therefore, it deposited only on the surface of ZSM-5 zeolite. Moreover, the surface Ni metal was easily aggregated to form larger particle in high temperature caused the significant loss of Ni active sites resulting in the decrease of CH_4 and CO_2 conversions. However, after the ZSM-5 zeolite support was modified by SBA-15 mesoporous silica, the highest conversion of CH_4 was shown by Ni/ZSM-5–SBA-15 composites catalyst. For the CO_2 conversion results of Ni/SBA-15 and Ni/ZSM-5–SBA-15 catalysts, the trends were slightly differed. Although the CH_4 conversion of Ni/ZSM-5–SBA-15 composites catalyst was highest, the CO_2 conversion was much similar with Ni/SBA-15 catalyst except for the CO_2 conversion at operating temperature of 650°C. These difference of CH_4 and CO_2 conversion

results between Ni/ZSM-5, Ni/SBA-15 and Ni/ZSM-5–SBA-15 catalysts confirmed that the existence of ZSM-5 zeolite could affect the reaction mechanisms and then it was discussed in the next section.

2.2 The CO_2 hydrogenation with CH_4 performance discussion

From the CH_4 and CO_2 conversion results, the catalytic performance of Ni/ZSM-5, Ni/SBA-15 and Ni/ZSM-5–SBA-15 catalyst was discussed based on above-mentioned literature reviews as follow.

2.2.1 *The difference in CH_4 conversion*

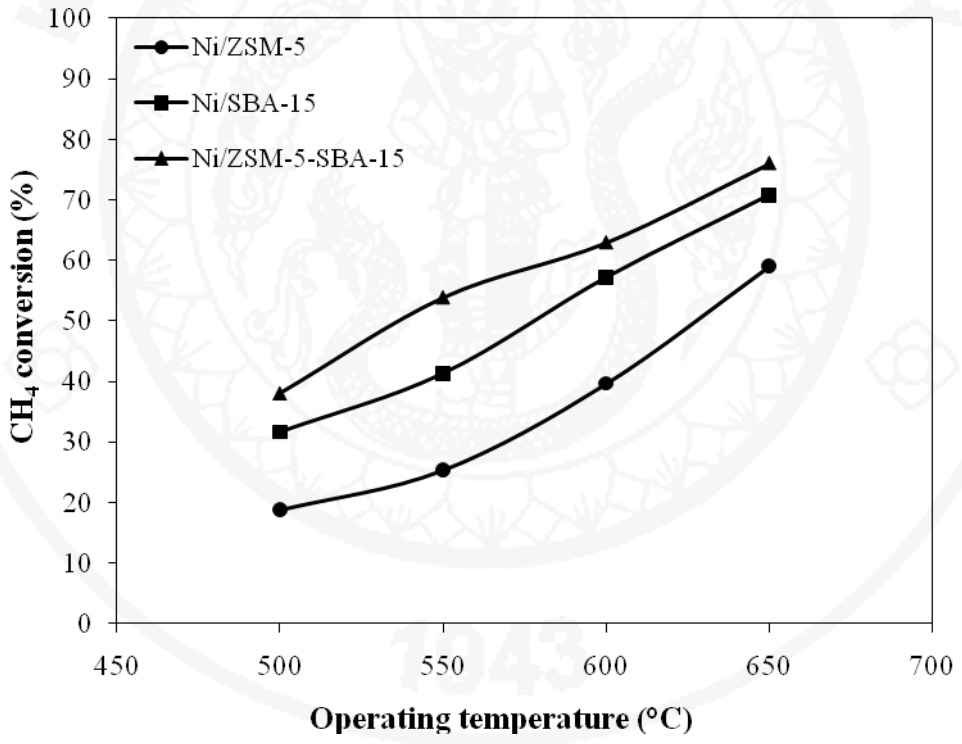

Figure 38 CH_4 conversion on various catalysts at CO_2/CH_4, 1; GHSV, 8,400 $mL \cdot h^{-1} g_{cat}^{-1}$; temperature, 500-650°C; pressure,1 atm; Ni loading, 5wt%.

Many researchers concerned that reaction on the heterogeneous catalysts involved with the existence of surface oxygen (Rostrup-nielsen and Hansen, 1993; Sun *et al.*, 2008; McGuire *et al.*, 2011). In CO_2 hydrogenation with CH_4, Cui *et*

al. (2007) reported that the surface oxygen produced from CO_2 decomposition reaction either on Ni or supports active sites in Eq.6 and Eq.7 could promote the CH_x oxidation reaction in Eq.8.

CO_2 decomposition; $CO_2 + *1 \rightarrow CO + O*1$ (6)

$CO_2 + *2 \rightarrow CO + O*2$ (7)

Oxidation of CH_x; $CH_x*1 + O*1 \rightarrow CO_2 + (x/2)H_2 + 2*1$ (8)

However, Ni metal was reported the low activity of CO_2 decomposition (Panov *et al.,* 1998). Therefore, the CO_2 decomposition reaction was mainly took place on the support active sites resulting in the many surface oxygen were existed on the support active sites and needed to exchange to Ni active sites that CH_x was mostly represented by surface oxygen exchange reaction in Eq.12 before oxidize.

Surface oxygen exchange; $O*2 + *1 \rightarrow O*1 + *2$ (12)

The surface oxygen exchange process was depended on the type of support and operating temperature. Martin and Duprez (1996) reported that the surface oxygen on SiO_2 support needed higher temperature (>650°C) than γ-Al_2O_3 support (~460°C) to diffuse on the support and change active sites with the metal. From this reason, the existence of ZSM-5 zeolite which was the crystal structure of SiO_2 and Al_2O_3 in Ni/ZSM-5–SBA-15 catalyst promoted the CH_x oxidation reaction resulting in the increase of CH_4 conversion.

2.2.2 *The difference in CO_2 conversion*

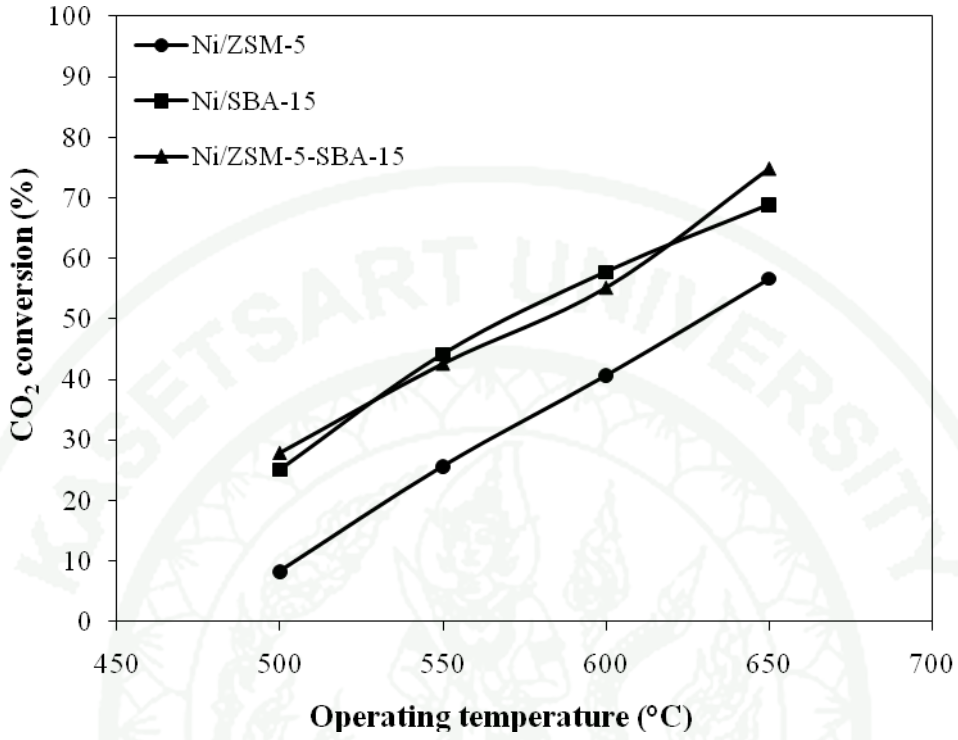

Figure 39 CO_2 conversion on various catalysts at CO_2/CH_4, 1; GHSV, 8,400 $mL \cdot h^{-1} g_{cat}^{-1}$; temperature, 500-650°C; pressure,1 atm; Ni loading, 5wt%.

Considering the CO_2 conversion in Figure 39, the similar results of Ni/SBA-15 and Ni/ZSM-5–SBA-15 were observed. Although the existence of ZSM-5 in Ni/ZSM-5–SBA-15 composites catalyst improved the CH_x oxidation reaction, this reaction produced CO_2. Moreover, it was reported by Chang *et al.* (1995) that the activation of methane with ZSM-5 support leaded to produce CO_2 as by product. Therefore, the CO_2 conversion was lower than CH_4 conversion on ZSM-5 based catalysts. In spite of the lower of CO_2 conversion than CH_4 conversion as in the low temperature range, the CO_2 conversion was significantly increased with operating temperature because some CO_2 were used by the RWGS reaction in Eq.12 that usually occurred in this temperature range as reported by many works (Chen and Cheng, 2002; Pinheiro *et al.*, 2009; Chen *et al*, 2010, 2011).

RWGS reaction; $CO_2 + H_2 \rightarrow H_2O + CO$ (12)

2.2.3 *CO yield*

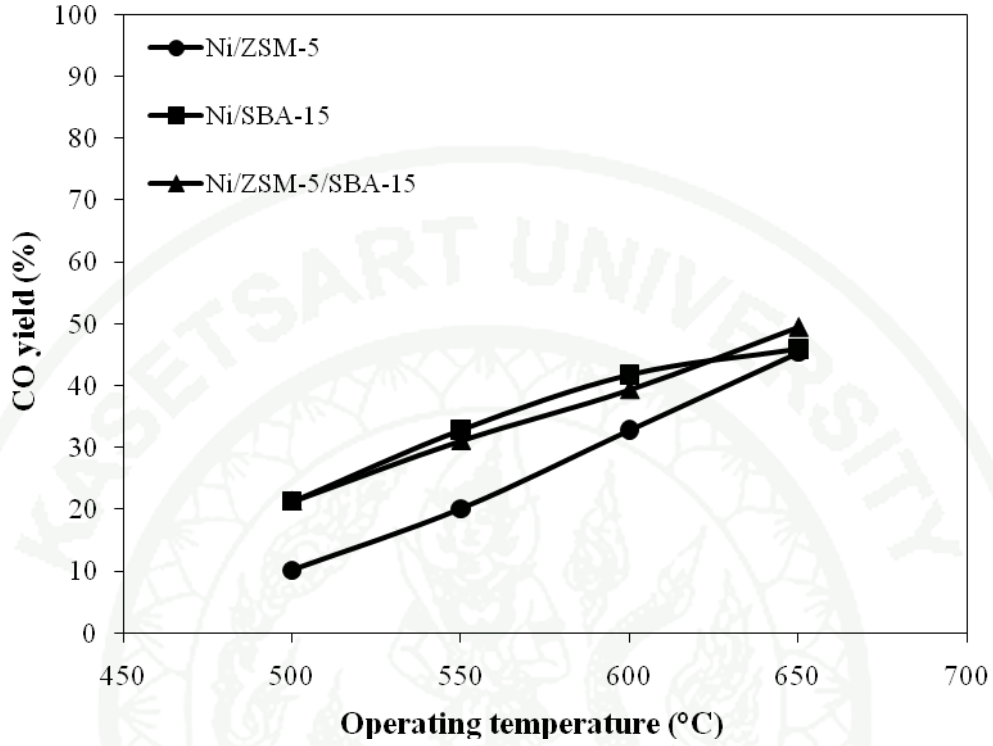

Figure 40 CO yield on various catalysts at CO_2/CH_4, 1; GHSV, 8,400 $mL \cdot h^{-1} g_{cat}^{-1}$; temperature, 500-650°C; pressure,1 atm; Ni loading, 5wt%.

The similar trend as CO_2 conversion was found in the CO yield as shown Figure 40. Although the acidity of ZSM-5 zeolite in Ni/ZSM-5−SBA-15 catalyst promoted the CH_4 dissociation and also the CH_4 conversion, the CO_2 conversion of Ni/SBA-15 and Ni/ZSM-5−SBA-15 were very similar, resulting in the resemblance yield of CO which was mainly generated from CO_2 as mentioned by Cui *et al.* (2007) in the literature review as shown in Eqs. 6-7 and Eq. 9.

CO_2 decomposition: $CO_2 + *1 \rightarrow CO + O*1$ (6)

$CO_2 + *2 \rightarrow CO + O*2$ (7)

Reforming reaction: $CH_x*1 + CO_2 + (x+1)*1 \rightarrow 2CO*1 + xH*1$ (9)

2.2.4 *Comparison of the performance with the other results*

According to the fact that many researchers have investigated the suitable catalysts for CO_2 hydrogenation with CH_4 reaction and some works also reported the catalytic performance of Ni/ZSM-5 (Chang *et al.*, 1996; Li *et al.*, 1998; Halliche *et al.*, 2008; Luengnaruemitchai and Kaengsilalai, 2008) and Ni/SBA-15 catalysts (Meili *et al.*, 2006; Liu *et al.*, 2009), the catalytic performance of catalysts used in this work has been compared with the other works as shown in Table 11.

Table 11 CH_4 conversion over Ni/ZSM-5 and Ni/SBA-15 catalysts (5wt%Ni loading)

Catalyst	Condition			Reference
	GHSV ($mL \cdot h^{-1} \cdot g_{cat}^{-1}$)	Temp. (°C)	CH_4 conversion (%)	
Ni/ZSM-5	8,400	650	59	This work
Ni/ZSM-5	60,000	700	78	Chang *et al.* (1996)
Ni/ZSM-5	-	800	87	Li *et al.* (1998)
Ni/ZSM-5	12,000	600	49	Halliche *et al.* (2008)
Ni/ZSM-5	30,000	700	91	Luengnaruemitchai and Kaengsilalai (2008)
Ni/SBA-15	8,400	650	71	This work
Ni/SBA-15	18,000	700	66	Meili *et al.* (2006)
Ni/SBA-15	50,000	600	35	Liu *et al.* (2009)

Although all catalysts used in this work were clearly examined and identified, the significant difference between our results and other results were observed. Unfortunately, there was still no evidence to confirm and explain these phenomena. These should be investigated for clearer understanding in the future.

CONCLUSION

In this work, ZSM-5–SBA-15 composites comprised of microporous structure of ZSM-5 zeolite and mesoporous structure of SBA-15 mesoporous silica was successfully synthesized by G-P123-HCl (UT) method. In order to obtain the complete structure of ZSM-5 zeolite in ZSM-5–SBA-15 composites, at least 7 h of the hydrothermal treatment time period was required. The template and high acid condition of SBA-15 mesoporous silica synthesis did not affect on the structure of ZSM-5 zeolite. Moreover, the uniformity of ZSM-5–SBA-15 composites structure depended on the particle size of ZSM-5 zeolite seeding. The smaller size of ZSM-5 zeolite seeding, more uniform structure of ZSM-5–SBA-15 composites was obtained. Therefore, ZSM-5 zeolite should be ground before use as the seeding.

After ZSM-5 zeolite, SBA-15 mesoporous silica and ZSM-5–SBA-15 composites supports were synthesized, the performance of catalysts in CO_2 hydrogenation with CH_4 of Ni/ZSM-5, Ni/SBA-15 and Ni/ZSM-5–SBA-15 catalysts were investigated. The lowest CH_4 and CO_2 conversion of Ni/ZSM-5 catalyst were observed due to the fact that its microporous structure was too small, leading to the deactivation by surface carbon species and aggregated Ni metals. The higher CH_4 conversion of Ni/SBA-15 catalyst was obtained according to the existence of SBA-15 mesoporous silica-promoted Ni dispersion. Ni/ZSM-5–SBA-15 catalyst exhibited the highest CH_4 conversion because the mesoporous structure of SBA-15 mesoporous silica promoted the Ni dispersion while ZSM-5 zeolite in the structure promoted the surface CH_x oxidation reaction. However, the surface CH_x oxidation reaction leaded to CO_2 gas production resulting in the resemblance of CO_2 conversion and also CO yield of Ni/SBA-15 and Ni/ZSM-5–SBA-15.

LITERATURE CITED

Anuwattana, R., K.J. Balkus, Jr., S. Asavapisit and P. Khummongkol. 2008. Conventional and microwave hydrothermal synthesis of zeolite ZSM-5 from the cupola slag. **Microporous and Mesoporous Materials** 111: 260-266.

Aparicio, P.F., M.F. Garcia, A.G. Ruiz and I.R. Ramos. 2000. Evaluation of the role of the metal–support interfacial centers in the dry reforming of methane on alumina-supported rhodium catalysts. **Journal of Catalysis** 190: 296-308.

Argauer, R.J. and G.R. Landolt. 1972. Crystalline zeolite ZSM-5 and method of preparing the same. **US patent** 3,702,886.

Ashcroft, A.T., A.K. Cheetham, M.L.H. Green and P.D.F. Vernon. 1991, Partial oxidation of methane to synthesis gas using carbon dioxide. **Nature** 352: 225-226.

Au, C.T. and H.Y. Wang. 1997. Mechanistic studies of methane partial oxidation to syngas over SiO_2-supported rhodium catalysts. **Journal of Catalysis** 167: 337-345.

Balat, M., M. Balat, E. Kurtay and H. Balat. 2009. Main routes for the thermo-conversion of biomass into fuels and chemicals. Part 2: Gasification systems. **Energy Conversion and Management** 50 (12): 3158-3168.

Bengaard, H. S., J.K. Nørskov, J. Sehested, B.S. Clausen, L.P. Nielsen, A.M. Molenbroek and J.R. Rostrup-Nielsen. 2002. Steam reforming and graphite formation on Ni catalysts. **Journal of Catalysis** 209: 365-384.

Bradford, M.C.J. and M.A. Vannice. 1998. CO_2 reforming of CH_4 over supported Pt catalysts. **Journal of Catalysis** 173: 157-171.

Burkett, S.L. and M.E. Davis. 1994. Mechanism of structure direction in the synthesis of Si-ZSM-5: An investigation by intermolecular ^{1}H-^{29}Si CP MAS NMR. **Journal of Physical Chemistry** 98 (17): 4647-4653.

_____ and _____. 1995. Mechanism of structure direction in the synthesis of pure-silica zeolites. 1. Synthesis of TPA/Si-ZSM-5. **Chemistry of Materials** 7 (5): 920-928.

_____ and _____. 1995. Mechanism of structure direction in the synthesis of pure-silica zeolites. 2. Hydrophobic hydration and structural specificity. **Chemistry of Materials** 7 (8): 1453-1463.

Campos, A.A., L. Dimitrov, C.R. da Silva, M. Wallau and E.A.U. González. 2006. Recrystallisation of mesoporous SBA-15 into microporous ZSM-5. **Microporous and Mesoporous Materials** 95: 92-103.

Čejka, J. and S. Mintova. 2007. Perspectives of micro/mesoporous composites in catalysis. **Catalysis Reviews: Science and Engineering** 49 (4): 457-509.

Chang, C.D. and A.T. bell. 1991. Studies on the mechanism of ZSM-5 formation. **Catalysis Letters** 8: 305-316.

Chang, J.S., S.E. Park and H. Chon. 1996. Catalytic activity and coke resistance in the carbon dioxide reforming of methane to synthesis gas over zeolite-supported Ni catalysts. **Applied Catalysis A: General** 145: 111-124.

Chang, Y.F., G.A. Somojai and H. Heinemann. 1995. An $^{18}O_2$ temperature-programmed isotope exchange study of transition-metal-containing ZSM-5 Zeolites used for oxydehydrogenation of ethane. **Journal of Catalysis** 154 (1): 24-32.

Chareonpanich, M., A. Nanta-ngern and J. Limtrakul. 2007. Short-period synthesis of ordered mesoporous silica SBA-15 using ultrasonic technique. **Materials Letters** 61 (29): 5153–5156.

_____, T. Namto, P. Kongkachuichay and J. Limtrakul. 2007. Synthesis of ZSM-5 zeolite from lignite fly ash and rice husk ash. **Fuel Processing Technology** 85 (25): 1623–1634.

Chen, C.S., J.H. Lin, J.H. You and K.H. Yang. 2010. Effects of potassium on Ni−K/Al_2O_3 catalysts in the synthesis of carbon nanofibers by catalytic hydrogenation of CO_2. **Journal of Physical Chemistry A** 114 (11): 3773-3781.

_____, J.H. You and C.C. Lin. 2002. Study on the Mechanism of CO Formation in Reverse Water Gas Shift Reaction Over Cu/SiO_2 Catalyst by Pulse Reaction, TPD and TPR. **Catalysis Letters** 83: 121-126.

_____, _____and _____. 2011. Carbon Nanofibers Synthesized from Carbon Dioxide by Catalytic Hydrogenation on Ni−Na/Al_2O_3 Catalysts. **Journal of Physical Chemistry C** 115 (5): 1464-1473.

Corma, A. 1995. Inorganic solid acids and their use in acid-catalyzed hydrocarbon reactions. **Chemical reviews** 95: 559-614.

_____. 1997. From microporous to mesoporous molecular sieve materials and their use in catalysis. **Chemical reviews** 97: 2373-2419.

_____, M. J. Díaz-Cabañas, J.L. Jordá, C. Martínez and M. Moliner. 2006. High-throughput synthesis and catalytic properties of a molecular sieve with 18- and 10-member rings. **Nature** 443: 842-845.

Corma, A, M. J. Díaz-Cabañas, F. Rey, S. Nicolopoulus and K. Boulahya. 2004. ITQ-15: The first ultralarge pore zeolite with a bi-directional pore system formed by intersecting 14-and 12-ring channels, and its catalytic implications. **Chemical Communications:** 1356-1357.

_____,_____, J. Martínez-Triguero, F. Rey and J. Rius. 2002. A large-cavity zeolite with wide pore windows and potential as an oil refining catalyst. **Nature** 418:514-517.

Cui, Y., H. Zhang, H. Xu and W. Li. 2007. Kinetic study of the catalytic reforming of CH_4 with CO_2 to syngas over Ni/α-Al_2O_3 catalyst: The effect of temperature on the reforming mechanism. **Applied Catalysis A: General** 318: 79-88.

Davis, M.E. 1991. Zeolites and molecular sieves: Not just ordinary catalysts. **Industrial & Engineering Chemistry Research** 30: 1675-1683.

_____, R.F. Lobo. 1992. Zeolite and molecular sieve synthesis. **Chemistry of Materials** 4: 756-768.

Didenko, L.P., V.I Savchenko, V.S. Arutyunov and L.A. Sementsova. 2008. Steam reforming of methane mixtures with ethylene over an industrial nickel catalyst. **Petroleum Chemistry** 48: 22-27

Edwards, J.H. and A.M. Maitra. 1995. The chemistry of methane reforming with carbon dioxide and its current and potential applications. **Fuel Processing Technology** 42: 269-289.

Freyhardt, C.C., M. Tsapatsis, R.F. Lobo, K.J. Balkus Jr and M. E. Davis. 1996. A high-silica zeolite with a 14-tetrahedral-atom pore opening. **Nature** 381(6580): 295-298.

Ginsburg, J.M., J. Pina, T.E. Solh and H.I. de Lasa. 2005. Coke formation over a nickel catalyst under methane dry reforming conditions: Thermodynamic and kinetic models. **Industrial & Engineering Chemistry Research** 44: 4846-4854.

Groen, J.C., J.A. Moulijna and J. Pérez-Ramírez. 2006. Desilication: on the controlled generation of mesoporosity in MFI zeolites. **Journal of Materials Chemistry** 16: 2121-2131.

Guari, Y., C. Thieuleux, A. Mehdi, C. Reye, R.J.P. Corriu, S. Gomez-Gallardo, K. Philippot, B. Chaudret and R. Dutartre. 2001. In-situ formation of gold nanoparticles within functionalized ordered mesoporous silica via an organometallic chimie douce approach. **Chemical Communications** 1374-1375.

Halliche, D., O. Cherifi, Y. B. Taarit and A. Auroux. 2007. Catalytic reforming of methane by carbon dioxide over nickel-exchanged zeolite catalysts. **Kinetics and Catalysis** 49: 667-675.

Hu, Y.H. and E. Ruckenstein. 1996. Transient kinetic studies of partial oxidation of CH_4. **Journal of Catalysis** 158: 260-266.

Khodakov, A.Y., V.L., Zholobenko, R. Bechara and D. Durand. 2005. Impact of aqueous impregnation on the long-range ordering and mesoporous structure of cobalt containing MCM-41 and SBA-15 materials. **Microporous and Mesoporous Materials** 79: 29-39.

Konya, Z., V.F. Puntes, I. Kiricsi, J. Zhu, P. Alivisatos and G.A. Somorjai. 2002. Novel two-step synthesis of controlled size and shape platinum nanoparticles encapsulated in mesoporous silica. **Catalysis Letters** 81: 137-140.

Kustova, M., K. Egeblad, K. Zhu and C.H. Christensen. 2007. Versatile route to zeolite single crystals with controlled mesoporosity: in situ sugar decomposition for templating of hierarchical zeolites. **Chemistry of Materials** 19: 2915-2917.

Li, W.Y., J. Feng and K.C. Xie. 1998. Ni/ZSM-5 catalyst for CH_4 reforming with CO_2. **Petroleum Science and Technology** 16: 539-553.

Liang, D.T. and D.W. Readey. 2005. Dissolution kinetics of crystalline and amorphous silica in hydrofluoric-hydrochloric acid mixtures. **Journal of the American Ceramic Society** 70 (8): 570-577.

Lin, J.C. and M.Z. Yates. 2005. Altering the crystal morphology of silicalite-1 through microemulsion-based synthesis. **Langmuir** 21: 2117-2120.

Liu, D., X.Y. Quek, H.H.A. Wah, G. Zeng, Y. Li and Y. Yang. 2009. Carbon dioxide reforming of methane over nickel-grafted SBA-15 and MCM-41 catalysts. **Catalysis Today** 148: 243–250.

Lu, G.Q. and S. Wang. 1999. Ni-based catalysts for carbon dioxide reforming of methane. **Chemical Technology** 29: 37-43.

Luengnaruemitchai, A. and A. Kaengsilalai. 2008. Activity of different zeolite-supported Ni catalysts for methane reforming with carbon dioxide. **Chemical Engineering Journal** 144: 96-102.

Mark, M.F. and W.F. Maier. 1996. CO_2 reforming of methane on supported Rh and Ir catalysts. **Journal of Catalysis** 164: 122-130.

Martin, D. and D. Duprez. 1996. Mobility of Surface Species on Oxides. 1. Isotopic Exchange of $^{18}O_2$ with ^{16}O of SiO_2, Al_2O_3, ZrO_2, MgO, CeO_2, and CeO_2-Al_2O_3. Activation by noble metals. Correlation with oxide basicity. **Journal of Physical Chemistry** 100 (22): 9429-9438.

McCusker, L.B. and C. Baerlocher. 2007. Chapter 2 Zeolite structures. **Studies in Surface Science and Catalysis** 168: 13-37.

McGuire, N.E., N.P. Sullivan, O. Deutschmann, H. Zhu and R.J. Kee. 2011. Dry reforming of methane in a stagnation-flow reactor using Rh supported on strontium-substituted hexaaluminate. **Applied Catalysis A: General** 394 (1-2): 257-265.

Meili, Z., J. Shengfu, H. Linhua, Y. Fengxiang, L. Chengyue and L. Hui. 2006. Structural characterization of highly stable Ni/SBA-15 catalyst and its catalytic performance for methane reforming with CO_2. **Chinese Journal of Catalysis** 27 (9): 777-782.

Meynen, V., P. Cool, E.F. Vansant, P. Kortunov, F. Grinberg, J. Kärger, M. Mertens, O.I. Lebedev and G. van Tendeloo. 2007. Deposition of vanadium silicalite-1 nanoparticles on SBA-15 materials. Structural and transport characteristics of SBA-VS-15. **Microporous and Mesoporous Materials** 99 (1-2): 14-22.

Mirji, S.A., S.B. Halligudi, N. Mathew, N.E. Jacob, K.R. Patil and A.B. Gaikwad. 2007. Adsorption of methanol on mesoporous SBA-15. **Material Letters** 61:88-92.

Nanta-Ngern, A. 2005. **The Synthesis of SBA-15 Mesoporous Silica from Rice Husk Ash.** M.S. Thesis, Kasetsart University.

Ogura, M., Y. Zhang, S.P. Elangovan and T. Okubo. 2007. Formation of ZMM-*n*: The composite materials having both natures of zeolites and mesoporous silica materials. **Microporous and Mesoporous Materials** 101: 224-230.

Oudejans, J.C. 1984. **Zeolite Catalyst in Some Organic Reactions**. n.p.

Panov, G.I., A.K. Uriarte, M.A. Rodkin and V.I. Sobolev. 1998. Generation of active oxygen species on solid surfaces. Opportunity for novel oxidation technologies over zeolites. Catalysis Today 41 (4): 365-385

Panpa, W. and S. Jinawath. Synthesis of ZSM-5 zeolite and silicalite from rice husk ash. **Applied Catalysis B: Environmental** 90 (3-4): 389-394.

Pinheiro, A.L., A.N. Pinheiro, A. Valentini, J.M Filho, F.F. de Sousa, J.R. de Sousa, 3, M.G.C. Rocha, 4, P. Bargiela and A. C. Oliveira. 2009. Analysis of coke deposition and study of the structural features of MAl_2O_4 catalysts for the dry reforming of methane. **Catalysis Communications** 11 (1): 11-14.

Pérez-Ramírez, J., C.H. Christensen, K. Egeblad, C.H. Christensen and J.C. Groen 2008. Hierarchical zeolites: enhanced utilisation of microporous crystals in catalysis by advances in materials design. **Chemical Society Reviews** 37: 2530-2542.

Rostrup-nielsen J.R. and J.H.B Hansen. 1993. CO_2-Reforming of Methane over Transition Metals. **Journal of Catalysis** 144 (1): 38-49.

Schüth, F. 2003. Endo- and exotemplating to create high-surface-area inorganic materials. **Angewandte Chemie** 42: 3604-3622.

Solymosi, F., A. Szőke and L. Egri. 1999. Decomposition of methane and its reaction with CO_2 over Rh/ZSM-5 catalyst. **Topics in Catalysis** 8: 249-257.

Sun, G.B., K. Hidajat, X.S. Wu and S. Kawi. 2008. A crucial role of surface oxygen mobility on nanocrystalline Y_2O_3 support for oxidative steam reforming of ethanol to hydrogen over Ni/Y_2O_3 catalysts. **Applied Catalysis B: Environmental** 81 (3-4): 303-312.

Takahashi, R., S. Sato, S. Tomiyama, T. Ohashi and N. Nakamura. 2007. Pore structure control in Ni/SiO_2 catalysts with both macropores and mesopores. **Microporous and Mesoporous Materials** 98 (1-3): 107-114.

Tang, S.B., F.L. Qiu and S.J. Lu. 1995. Effect of supports on the carbon deposition of nickel catalysts for methane reforming with CO_2. **Catalysis Today** 24: 253-255.

Tao, Y., H. Kanoh, L. Abrams and K. Kaneko. 2006. Mesopore-modified zeolites: Preparation, characterization, and applications. **Chemical reviews** 106: 896-910.

Tomishige, K., Y.G. Chen and K. Fujimoto. 1999. Studies on carbon deposition in CO_2 reforming of CH_4 over nickel–magnesia solid solution catalysts. **Journal of Catalysis** 181: 91–103.

_____, O.Yamazaki, Y. Chen, K. Yokoyama, X. Li and K. Fujimoto. 1998. Development of ultra-stable Ni catalysts for CO_2 reforming of methane. **Catalysis Today** 45: 35-39.

Tsipouriari, V.A. and X.E. Verykios. 1998. Catalytic partial oxidation of methane to synthesis gas over Ni-based catalysts. **Journal of Catalysis** 179: 292-299.

Treacy, M.M.J. and J.B. Higgins. 2001. **Collection of Simulated XRD Powder Patterns for Zeolites**. n.p.

Wang, S. and G.Q. Lu. 1998. Catalytic activities and coking characteristics of oxides-supported Ni catalysts for CH_4 reforming with carbon dioxide. **Energy & Fuels** 12: 248-256.

_____, _____ and G.J. Millar. 1996. Carbon dioxide reforming of methane to produce synthesis gas over metal-supported catalysts: state of the art. **Energy & Fuels** 10: 896-904.

Yu, J. Chapter 3 Synthesis of zeolites. 2007. **Studies in Surface Science and Catalysis** 168: 39-103.

Zhang,W.D., B.S. Liu, C. Zhu and Y.L. Tian. 2005. Preparation of La_2NiO_4/ZSM-5 catalyst and catalytic performance in CO_2/CH_4 reforming to syngas. **Applied Catalysis A: General** 292: 138-143.

Zhang, Z.L., V.A. Tsipouriari, A.M. Efstathiou and X.E. Verykios 1996. Reforming of methane with carbon dioxide to synthesis gas over supported rhodium catalysts I. Effects of support and metal crystallite size on reaction activity and deactivation characteristics. **Journal of catalysis** 158: 51-63.

Zhao, D., J. Feng, Q. Huo, N. Melosh, G.H. Fredrickson, B.F. Chmelka and G.D. Stucky. 1998. Triblock copolymer syntheses of mesoporous silica with periodic 50 to 300 angstrom pores. **Science** 279: 548-552.

_____, Q. Huo, J. Feng, B.F. Chmelka, and G.D. Stucky. 1998. Nonionic Triblock and Star Diblock Copolymer and Oligomeric Surfactant Syntheses of Highly Ordered, Hydrothermally Stable, Mesoporous Silica Structures. **Journal of the American Chemical Society** 120: 6024-6032.

Zholobenko, V.L., A. Evans, D. Plant and S.M. Holmes. 2001. Acid sites in mesoporous materials: a DRIFTS study. **Microporous and Mesoporous Materials** 44-45: 793-799.

_____, V.L, A.Y. Khodakov, M. Impéror-Clerc, D. Durand and I. Grillo. 2008. Initial stages of SBA-15 synthesis: An overview. **Advances in Colloid and Interface Science** 142: 67-74.

APPENDICES

Appendix A

Qualitative and Quantitative Results from Gas Chromatography

Quantitative and Qualitative Results from Gas Chromatography

Gas chromatography was performed in a specially designed instrument. The major instrumental components consisted of a flowing mobile phase, an injector port, a separation column containing the stationary phase, a detector, and a data recording system as shown in Appendix Figure A1. Certain amount of gaseous mixture, 1.0 mL in this research, was injected into gas chromatograph at the injector port and was volatilized in a hot injection chamber before it was transported to the head of the chromatic column. Then, a flow of inert carrier gas (as a mobile phase) swept the injected mixture through a heated column which contained the stationary phase. The gaseous sample moved along the packing column whereas its component gas moved with different flow rates and thus separated into pure component. Before each component exited the instrument, it passed through a detector. The detector sent an electronic signal to the recorder and the analyzed results were printed out.

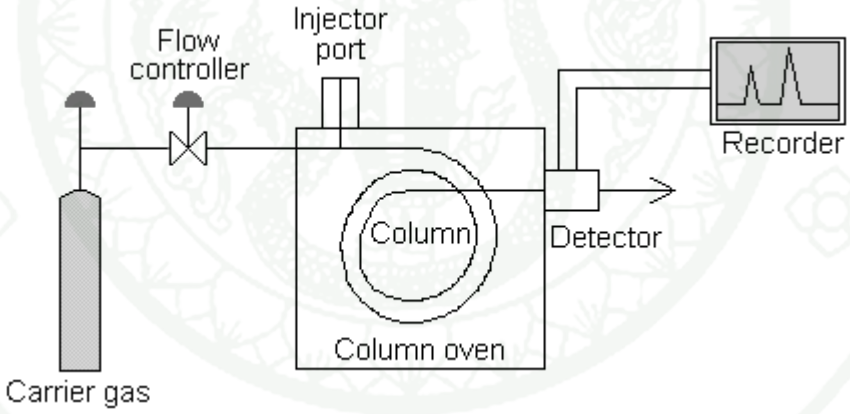

Appendix Figure A1 Schematic diagram of gas chromatograph.

In this work, the quantitative and qualitative data of product composition was obtained from TCD-GC gas chromatography as mention in the experimental chapter. Before analysis, the condition of operation was set and kept on running for about an hour to stabilize the based line. Certain volume of sample mixture (1.0 mL in this case) was injected into the injection port by gas syringe. After the mixture of sample gas was analyzed, the qualitative and quantitative data were interpreted from the peak area obtained from the recorder. The component of injected gas mixture can be

identified by using the value of retention time data compared with the retention time received from injected standard gas. The chromatogram of standard gases and liquids used in this research were shown as following figures:

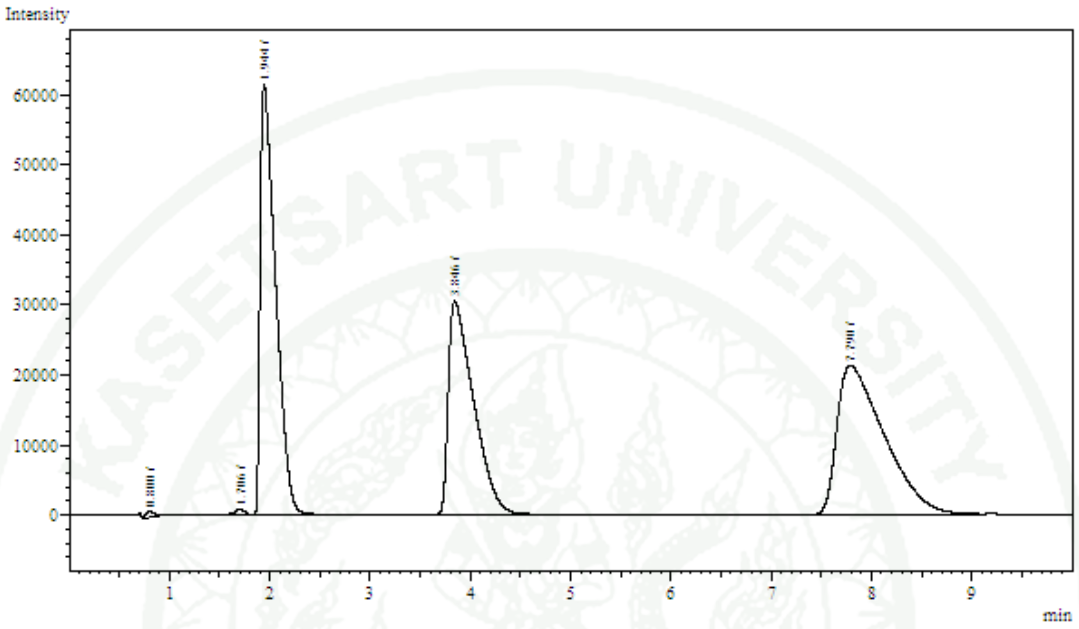

Appendix Figure A2 Chromatogram of standard gases for H_2, CO, CH_4 and CO_2.

The quantitative analysis of gas sample was obtained from the calibration curves where the correlation between the amount of injected gas sample (mole) and the peak area of gas chromatograms were proposed. The correlation between these parameters (mole and area) was analyzed by a linear regression equation. All the calibration curves for each single standard gas and liquid used in this research were shown in Appendix Table A1.

Appendix Table A1 Equation of calibration curves for standard gas

Substance	Equation	R^2
H_2	mol = (area x 10^{-9}) - (7 x 10^{-7})	0.9734
CO	mol = (area x 2 x 10^{-11}) + (2 x 10^{-7})	0.9997
CO_2	mol = (area x 10^{-11}) + (3 x 10^{-7})	0.9996
CH_4	mol = (area x 2 x 10^{-11}) + (2 x 10^{-7})	0.9997

The calculation for the amount of each component in a standard-gas mixture can be calculated as follows:

$$Amount\ of\ component_i\ (mol) = \frac{V_i}{100 \times 22{,}400}$$

where V_i = % volume of component$_i$ (cm^3/cm^3)

T = volume of standard gases mixture (mL)

The amount of outlet gases (mole) in Ni/ZSM-5, Ni/SBA-15 and Ni/ZSM-5−SBA-15 catalysts were shown in Appendix Table A2-A4.

Appendix Table A2 Amount of outlet gases obtained from Ni/ZSM-5 catalyst

Temp. (°C)	GHSV ($mL \cdot h^{-1} \cdot g_{cat}^{-1}$)	mol_{out}			
		CH_4	CO_2	H_2	CO
500	24,000	1.96E-05	1.44E-05	-	2.36E-06
	18,000	1.91E-05	1.4E-05	-	2.71E-06
	12,000	1.77E-05	1.46E-05	-	3.21E-06
	8,400	1.71E-05	1.43E-05	-	3.72E-06
550	24,000	1.74E-05	1.29E-05	1.186E-06	4.74E-06
	18,000	1.72E-05	1.28E-05	1.428E-06	5.37E-06
	12,000	1.65E-05	1.22E-05	1.878E-06	6.47E-06
	8,400	1.57E-05	1.16E-05	2.346E-06	7.37E-06
600	24,000	1.61E-05	1.12E-05	2.508E-06	8.05E-06
	18,000	1.51E-05	1.05E-05	2.852E-06	9.09E-06
	12,000	1.35E-05	1E-05	3.411E-06	1.08E-05
	8,400	1.27E-05	9.24E-06	3.684E-06	1.2E-05
650	24,000	1.34E-05	8.97E-06	0.00000375	1.23E-05
	18,000	1.21E-05	8.25E-06	3.735E-06	1.34E-05
	12,000	1.05E-05	7.48E-06	2.797E-06	1.5E-05
	8,400	8.63E-06	6.75E-06	2.999E-06	1.66E-05

Appendix Table A3 Amount of outlet gases obtained from Ni/SBA-15 catalyst

Temp. (°C)	GHSV ($mL \cdot h^{-1} \cdot g_{cat}^{-1}$)	mol_{out}			
		CH_4	CO_2	H_2	CO
500	24,000	1.78E-05	1.25E-05	1.11E-06	4.83E-06
	18,000	1.73E-05	1.22E-05	1.45E-06	5.43E-06
	12,000	1.54E-05	1.26E-05	1.85E-06	6.51E-06
	8,400	1.44E-05	1.17E-05	2.68E-06	7.82E-06
550	24,000	1.44E-05	9.99E-06	3.32E-06	9.59E-06
	18,000	1.38E-05	9.6E-06	3.56E-06	1.02E-05
	12,000	1.31E-05	8.99E-06	3.94E-06	1.14E-05
	8,400	1.24E-05	8.69E-06	4.03E-06	1.21E-05
600	24,000	1.16E-05	8.01E-06	2.45E-06	1.27E-05
	18,000	1.05E-05	7.63E-06	2.63E-06	1.35E-05
	12,000	9.84E-06	7.19E-06	2.66E-06	1.43E-05
	8,400	9.03E-06	6.57E-06	2.08E-06	1.53E-05
650	24,000	8.56E-06	5.11E-06	2.78E-06	1.72E-05
	18,000	7.84E-06	4.72E-06	3.22E-06	1.71E-05
	12,000	6.46E-06	4.63E-06	3.04E-06	1.78E-05
	8,400	6.16E-06	4.84E-06	4.24E-06	1.68E-05

Appendix Table A4 Amount of outlet gases obtained from Ni/ZSM-5−SBA-15 catalyst

Temp. (°C)	GHSV ($mL \cdot h^{-1} \cdot g_{cat}^{-1}$)	mol_{out}			
		CH_4	CO_2	H_2	CO
500	24,000	1.45E-05	1.11E-05	3.42E-06	7.36E-06
	18,000	1.44E-05	1.1E-05	3.14E-06	7.51E-06
	12,000	1.35E-05	1.11E-05	3.52E-06	7.74E-06
	8,400	1.31E-05	1.12E-05	3.53E-06	7.82E-06
550	24,000	1.09E-05	9.13E-06	2.5E-06	1.08E-05
	18,000	1.08E-05	8.72E-06	2.53E-06	1.08E-05
	12,000	1.02E-05	8.76E-06	2.42E-06	1.11E-05
	8,400	9.72E-06	8.92E-06	2.45E-06	1.14E-05
600	24,000	1.01E-05	6.99E-06	2.6E-06	1.37E-05
	18,000	9.21E-06	6.71E-06	3.49E-06	1.42E-05
	12,000	8.45E-06	6.77E-06	3.91E-06	1.41E-05
	8,400	7.81E-06	6.97E-06	4.48E-06	1.44E-05
650	24,000	6.17E-06	4.53E-06	8.24E-06	1.65E-05
	18,000	6.59E-06	4.09E-06	8.3E-06	1.66E-05
	12,000	6.06E-06	3.78E-06	9.4E-06	1.73E-05
	8,400	5.05E-06	3.9E-06	9.22E-06	1.81E-05

Appendix B

Conversion and Yield Results

Conversion and Yield Results

The calculation for the conversions of CH_4 and CO_2 to H_2 and CO products in CO_2 reforming with CH_4 reaction is shown as follows:

Percentage of CH_4 conversion:

$$CH_4\ conversion\ (\%) = \frac{CH_{4,in} - CH_{4,out}}{CH_{4,in}} \times 100\%$$

Percentage of CO_2 conversion:

$$CO_2\ conversion\ (\%) = \frac{CO_{2,in} - CO_{2,out}}{CO_{2,in}} \times 100\%$$

Percentage yield of H_2 products:

$$H_2\ yield(\%) = \frac{H_{2,out}}{2CH_{4,in}} \times 100\%$$

Percentage yield of CO products:

$$CO\ yield(\%) = \frac{CO_{out}}{CH_{4,in} + CO_{2,in}} \times 100\%$$

The examples of calculation for the CH_4 and CO_2 conversions and H_2 and CO yield can be shown as following table:

Appendix Table B1 Calculation of CH_4 and CO_2 conversions and H_2 and CO yield in CO_2 reforming with CH_4 reaction over Ni/ SBA-15 catalyst

Description	Calculation
CO_2 reforming with CH_4 reaction at GHSV = 8,400 mLh^{-1} g_{cat}^{-1}, T = 550°C, P = 1 atm	
Inlet: Peak area of CH_4	1,043,857
$CH_{4,in}$ amount	2.108×10^{-5}
Outlet: Peak areas of CH_4	608,749
$CH_{4,out}$ amount	1.237×10^{-6}
CH_4 conversion	41.29 %
Inlet: Peak area of CO_2	1,525,905
$CO_{2,in}$ amount	1.556×10^{-5}
Outlet: Peak areas of CO_2	838,654
$CO_{2,out}$ amount	8.990×10^{-6}
CO_2 conversion	44.17 %
Outlet: Peak areas of H_2	4,725
H_2 amount	4.025×10^{-6}
H_2 yield	9.55 %
Outlet: Peak areas of CO	602,468
CO amount	1.20×10^{-5}
CO yield	32.91 %

Appendix C

X-ray Diffraction of ZSM-5 Zeolite

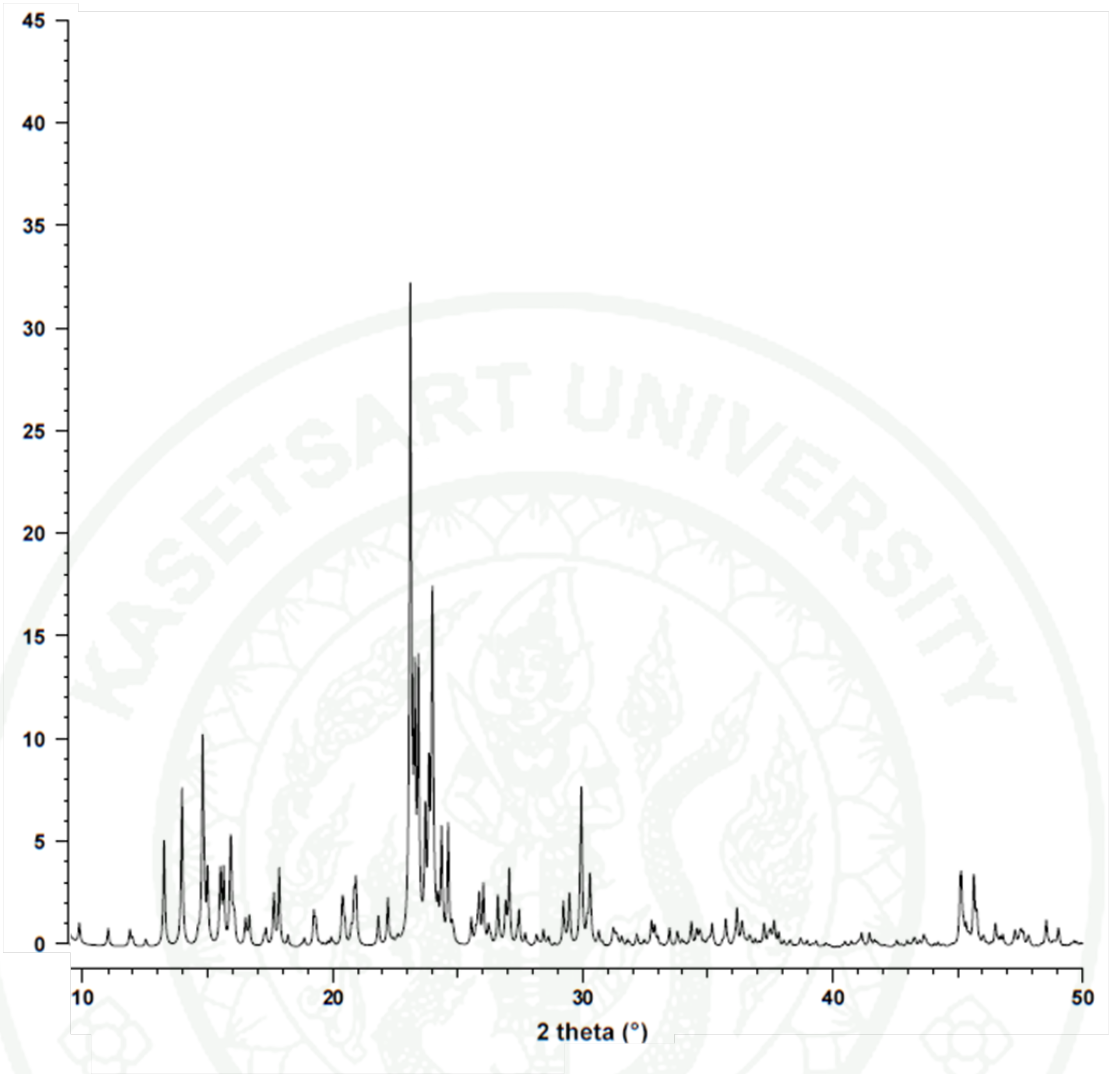

Appendix Figure C1 X-ray diffraction of ZSM-5 zeolite.

Source: Treacy and Higgins (2001)

CIRRICULUM VITAE

NAME : Mr. Thammachat Metchanan

BIRTH DATE : January 26, 1985

BIRTH PLACE : Nakhon Ratchasima, Thailand

EDUCATION :

YEAR	**INSTITUTE**	**DEGREE**
2008	KasetsartUniv.	B.Sc.(Industrial Chem.)
2011	Kasetsart Univ.	M.Eng.(Chemical)

SCHOLARSHIP : Teacher Assistant Scholarship from ADB Program of Department of Chemical Engineering, Kasetsart University 2008-2009